Using Raman spectroscopy to characterize biological materials

Article *in* Nature Protocols · March 2016

DOI: 10.1038/nprot.2016.036

14 authors, including:

Holly Butler
University of Strathclyde
19 PUBLICATIONS **725** CITATIONS
SEE PROFILE

Lorna Ashton
Lancaster University
39 PUBLICATIONS **919** CITATIONS
SEE PROFILE

Benjamin Bird
Becton, Dickinson and Company (BD)
55 PUBLICATIONS **1,358** CITATIONS
SEE PROFILE

Gianfelice Cinque
Diamond Light Source
179 PUBLICATIONS **2,153** CITATIONS
SEE PROFILE

Using Raman spectroscopy to characterize biological materials

Holly J Butler[1,2], Lorna Ashton[3], Benjamin Bird[4], Gianfelice Cinque[5], Kelly Curtis[6], Jennifer Dorney[6], Karen Esmonde-White[7], Nigel J Fullwood[8], Benjamin Gardner[6], Pierre L Martin-Hirsch[1,9], Michael J Walsh[10,11], Martin R McAinsh[1], Nicholas Stone[6,12] & Francis L Martin[1]

[1]Lancaster Environment Centre, Lancaster University, Lancaster, UK. [2]Centre for Global Eco-Innovation, Lancaster Environment Centre, Lancaster University, Lancaster, UK. [3]Department of Chemistry, Lancaster University, Lancaster, UK. [4]Daylight Solutions, San Diego, California, USA. [5]Diamond Light Source, Harwell Science and Innovation Campus, Chilton, Oxfordshire, UK. [6]Department of Biomedical Physics, Physics and Astronomy, University of Exeter, Exeter, UK. [7]Department of Internal Medicine, University of Michigan Medical School, Ann Arbor, Michigan, USA. [8]Department of Biomedical and Life Sciences, School of Health and Medicine, Lancaster University, Lancaster, UK. [9]School of Pharmacy and Biomedical Sciences, University of Central Lancashire, Preston, UK. [10]Department of Pathology, University of Illinois at Chicago, Chicago, Illinois, USA. [11]Department of Bioengineering, University of Illinois at Chicago, Chicago, Illinois, USA. [12]Biophotonics Research Unit, Gloucestershire Hospitals NHS Foundation Trust, Gloucester, UK. Correspondence should be addressed to M.R.M. (m.mcainsh@lancaster.ac.uk), N.S. (n.stone@exeter.ac.uk) or F.L.M. (f.martin@lancaster.ac.uk).

Published online 10 March 2016; doi:10.1038/nprot.2016.036

Raman spectroscopy can be used to measure the chemical composition of a sample, which can in turn be used to extract biological information. Many materials have characteristic Raman spectra, which means that Raman spectroscopy has proven to be an effective analytical approach in geology, semiconductor, materials and polymer science fields. The application of Raman spectroscopy and microscopy within biology is rapidly increasing because it can provide chemical and compositional information, but it does not typically suffer from interference from water molecules. Analysis does not conventionally require extensive sample preparation; biochemical and structural information can usually be obtained without labeling. In this protocol, we aim to standardize and bring together multiple experimental approaches from key leaders in the field for obtaining Raman spectra using a microspectrometer. As examples of the range of biological samples that can be analyzed, we provide instructions for acquiring Raman spectra, maps and images for fresh plant tissue, formalin-fixed and fresh frozen mammalian tissue, fixed cells and biofluids. We explore a robust approach for sample preparation, instrumentation, acquisition parameters and data processing. By using this approach, we expect that a typical Raman experiment can be performed by a nonspecialist user to generate high-quality data for biological materials analysis.

INTRODUCTION

Raman microspectroscopy has been shown to be a powerful analytical technique in the study of biological materials, and it allows rapid, noninvasive and high spatial resolution acquisition of biochemical and structural information through the generation of point spectra or spectral images. Although it has been traditionally used for analytical chemistry applications, there has been a notable rise in the use of this technique within biological studies, particularly in the field of biomedicine[1–4].

Raman spectroscopy

Raman spectroscopy uses monochromatic light, often in the near-IR (NIR), visible or UV range, to exploit the phenomena of inelastic scattering, or Raman effect, that describes the excitation of photons to virtual energy states and the resultant loss (Stokes) or gain (anti-Stokes) of energy that occurs because of the interaction of light with vibrational modes associated with chemical bonds within the sample. This shift in energy is indicative of discrete vibrational modes of polarizable molecules, and thus a qualitative measurement of biochemical composition can be obtained. Raman spectra can infer quantitative information, provided that the instrument response function is adequately corrected. Typically, the significant regions of the Raman spectrum that are observed within biological specimens fall within 400–2,000 cm^{-1} wavenumbers, associated with bond vibrations of proteins (1,500–1,700 cm^{-1}), carbohydrates (470–1,200 cm^{-1}), phosphate groups of DNA (980, 1,080 and 1,240 cm^{-1}) and additional cellular biomolecules[1,5]. Higher-frequency bond vibrations associated with CH, NH and OH stretching in lipids and proteins can also be observed at higher wavenumbers (2,700–3,500 cm^{-1})[5]. Consequently, a distinctive biological 'fingerprint' is derived from the biological sample under investigation, and it can contribute to our understanding of the specimen. **Figure 1** illustrates the principle of elastic (Rayleigh) and inelastic scattering when analyzing biological specimens.

Raman spectroscopy has a high molecular specificity, making it an excellent technique for materials analysis. However, Raman scattering is a rare phenomenon with an exceptionally low probability of occurrence (~1 in 10^8) in comparison with its counterpart Rayleigh scattering, and thus it is typically described as an insensitive technique. Its increased applicability is largely attributed to the technological advancement of highly efficient laser sources, low-noise detectors, effective Rayleigh filters and high-throughput optics[6]. The development of microspectrometers, which combine the power of optical magnification and direct visualization of the sample, has also contributed to further exploitation in biological fields. Because of this, it is possible to not only derive single point spectra but also to produce highly informative Raman images of the sampling area with improved interpretability[7]. The ability to acquire high-quality spectra at subcellular resolution coupled with the capability to obtain valuable information noninvasively, label-free and without interference from water, makes Raman spectroscopy an ideal approach for *in vivo* biological investigations.

There are many factors that influence spectral resolution, which are outlined in detail in this protocol. The spatial resolution of optical Raman microspectroscopy is governed mainly by the diffraction limit of light, and therefore it is dependent on the laser wavelength (λ) in use, as well as on the numerical aperture (NA)

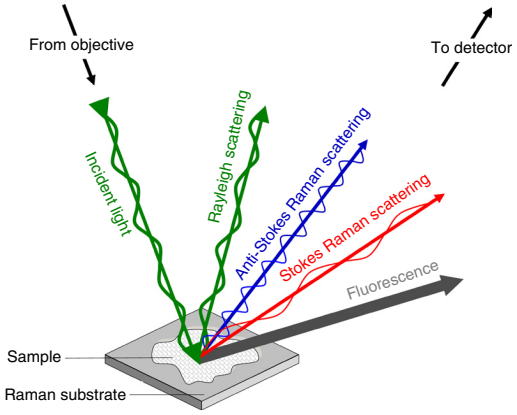

Figure 1 | Schematic identifying light scattering after laser exposure on a sample surface. Photons of light are focused on the sample through the microscope objective at a defined magnification. When they interact with chemical bonds within the biological specimen, electrons are excited to virtual energy levels. These biological molecules return to the original energy level by emitting a photon of light, known as elastic or Rayleigh scattering, or it can undergo an energy shift and return at lower (Stokes) or higher (anti-Stokes) energy levels, known as Raman scattering. Raman scattering is a low-probability process with around 1 in 10^8 photons inelastically scattered (arrow widths are not representative); Stokes Raman scattering is more intense than anti-Stokes scattering because of the increased probability of a molecule being in the ground vibrational state. Fluorescence can occur when electrons are excited to electronic energy levels and return to the ground energy level by emitting a photon of light at a longer wavelength.

of the objective. Theoretically, for a confocal microscope, the diffraction limit for visible (488 nm) to NIR (~1,033 nm) light, using long-working-distance to water- or oil-immersion objectives with NA values from 0.5 to 1.2, would be in the range of 0.2–1 µm. In practice, it is rarely possible to achieve the diffraction limit, owing to both imperfect optics and beam scattering at the interface of the sample. However, alternative sampling modes such as surface-enhanced Raman scattering (SERS) and tip-enhanced Raman spectroscopy (TERS) have been shown to provide spatial resolution below the diffraction limit, as targeted single-molecule detection is possible[8,9]. This is due to the interaction of biomolecules with roughened surfaces, such as metallic nanoparticles, that effectively enhance the electric field by a factor of up to 10^{14}. This is associated with the excitation of localized surface plasmons, which significantly enhance the local electric field of the light incident on the molecules adsorbed onto the metal surface. Furthermore, some small enhancement can originate from the charge transfer between the two materials.

A typical Raman study can rapidly accumulate a large, information-rich spectral data set. However, as this data set expands, the extraction of biological information becomes increasingly challenging. For this reason, multivariate analysis approaches are often used in order to effectively extricate the underlying chemical and structural information[10]. Spectral data sets often present a substantial computational burden, and thus analysis usually includes a data-reduction step, particularly as there are many covariant features in the spectra. This information can then be fed into unsupervised (clustering) or supervised classifications to differentiate individual spectra, which can then infer biological information[11]. Raman imaging (global illumination) and mapping (stepwise) have particularly benefited from these classification capabilities, as spectral discrimination is indicative of the underlying biological architecture, which has proved to be valuable in the field of cancer diagnosis, in which this approach has complemented conventional histopathological techniques[12].

Applications

Raman spectroscopy presents a method of sample examination with a high degree of flexibility, enabling data to be recorded from a diverse array of sample types including fixed, fresh or live tissues and cells. The application of Raman microspectroscopy to the characterization of biological materials is a rapidly expanding field, and it has been used in the fields of pharmacology[13–15], microbiology[16–20], toxicology[21,22], plant science[23–25] and human biology. Considerable advances have been made, particularly in regard to cancer diagnosis and prognosis[26]. Clinical implementation is firmly on the horizon[27], as spearheaded by recently formed networks such as 'Raman4Clinics' (http://www.raman4clinics.eu/) and Clinical Infrared and Raman Spectroscopy for Medical Diagnosis (CLIRSPEC; http://clirspec.org/). Raman spectroscopy and its derivatives, coupled with multivariate analysis, can classify neoplasia in brain[28–31], breast[32], bladder[33], colorectal[34,35], larynx[36], lung[37], lymph node[38,39], esophageal[40–42], prostate[43–46], and uterine and cervical[47–50] tissues using both point spectra and imaging approaches. These examples have used a range of sample formats, including fixed cells and tissues, *in vivo* measurements with advances in fiber optic attachments and spatially offset Raman spectroscopy (SORS), as well as noninvasive biofluid measurements[51]. In addition to cancer studies, the technique has been used to shed light on infectious diseases such as malaria[52–55]. Owing to the relatively fast sampling time and mapping ability of Raman microspectroscopy in aqueous environments, the 2D and 3D analysis of *in vitro* cell models is possible[56–59], which has been particularly useful in toxicology and therapeutic studies[60,61].

The application of SERS has been shown to vastly improve the spectral intensity obtained from typically weak Raman scatterers, such as dilute biofluids[62]. SERS has been used across a wide range of biomedical studies, including DNA and drug detection[63–66]. This approach has also been shown to overcome autofluorescence, which has often limited research capabilities in samples with intrinsic fluorescence, such as chlorophyll in plants, as this strong signal can often engulf the relatively rare Raman event[24]. Reduced Raman performance in plant research has markedly restricted its application in this area, with previous research focused on the quantification and identification of plant constituents[67–72], as well as the imaging of nonfluorescent tissues[25,73–75]. As fluorescence has a defined wavelength profile, it is also possible to overcome fluorescence by using alternative radiation sources using lasers at wavelengths that are outside typical biological matrix absorbance, e.g., in the NIR (1,064 nm) region[76]. Water has also been found to be a significant fluorescence quencher, which has benefited *in vivo* studies, as was recently demonstrated in fundamental plant monitoring[77,78].

Limitations

The molecular specificity of Raman spectroscopy is powerful for the study of biological materials. However, there are a number of disadvantages associated with the technique. As Raman scattering is a relatively low-probability event, low sensitivity can be an issue, which is exacerbated by interference from fluorescence[13]. Because of the intense laser powers typically used, local thermal decomposition of the sample may be encountered, especially

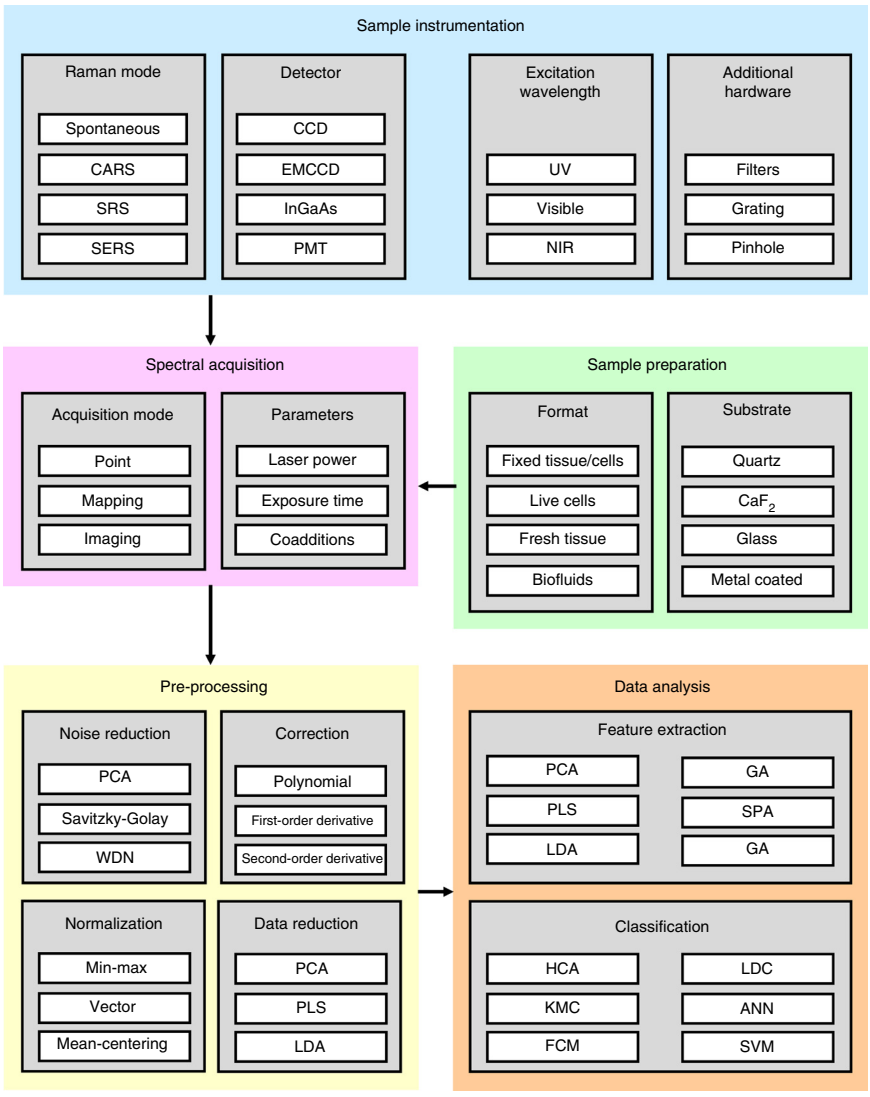

Figure 2 | Raman microspectroscopy workflow diagram highlighting the key aspects of experimental design including instrumentation, sample preparation, spectral acquisition and data processing with representative examples. It is not possible to conduct some options in combination, such as an InGaAs detector with UV wavelengths, and thus experimental design requires thorough planning before experimentation. Options provided are not exhaustive, and other alternatives are available. LDA, linear discriminant analysis; GA, genetic algorithm; SPA, sequential progression algorithm; HCA, hierarchical cluster analysis; KMC, *k*-means clustering; ANN, artificial neural networks.

when using UV or visible wavelengths. Sample burning (or photoablation) may be observed visibly by dark areas on the sample and spectroscopically by the presence of amorphous carbon bands (C=C, ~1,500 cm^{-1}) in the spectra, or saturation of the detector. The protocol described here will provide troubleshooting advice to avoid these particular issues. Fourier-transform IR (FTIR) spectroscopy is an alternative vibrational spectroscopy technique that is also suitable for the analysis of biological materials (for a recent protocol, see Baker *et al.*[79]). Although it is based on fundamentally different physical excitation processes, FTIR retains both molecular specificity and sensitivity, and thus it has been used to derive spectral data and elucidate biological information, complementary to Raman spectroscopy[80–82].

The aim of this article is to describe a specific protocol for Raman microspectroscopy that can be applied to a variety of biological samples independent of a specific manufacturer's instrumentation and software. The protocol will address (i) sample preparation, (ii) spectral acquisition and (iii) data analysis of spectral data sets, with anticipated results derived from a range of biological studies (**Fig. 2**). It is important to note that this technique can also be applied to nonbiological materials, providing insights into the steps involved in Raman studies. In this protocol, we approach principal aspects of planning and implementing Raman investigations that can be applied to a variety of biological samples. We direct the reader to additional protocols that approach specific biological applications[75,83–86]. It is our aim that by unifying protocols from leading researchers in the field, spectroscopists and biologists can build new interdisciplinary studies into biological samples incorporating Raman microspectroscopy into the suite of molecular biology tools.

Experimental design

In the PROCEDURE, we focus on four experimental examples: (i) *in vivo* spectral exploration of live plant samples (suitable for fresh tissue analysis); (ii) imaging of fixed human tissue; (iii) SERS classification of endometrial cancer using biofluids; and (iv) analysis of cultured mammalian cells. These examples encompass both point and image mapping acquisition approaches, while exploring a range of pre-processing and analysis steps including exploratory image processing and spectral classification. This section of the INTRODUCTION provides background on these steps and more detailed guidance on how to decide which of these approaches to take.

Experimental design: instrument options

Figure 3 presents an overview of a typical Raman system and identifies key instrumental components. There are numerous Raman spectroscopic variations available, as described in **Table 1**. This protocol will focus primarily on spontaneous Raman microspectroscopy, which is a standard approach that does not require additional instrumentation, unless otherwise stated.

Before setting up the instrument and starting the analysis (Step 3), you need to consider what scientific questions you are trying to answer and what types of samples you are going to be analyzing. In this protocol, we refer to two types of investigative aims: exploratory (where you are trying to find out

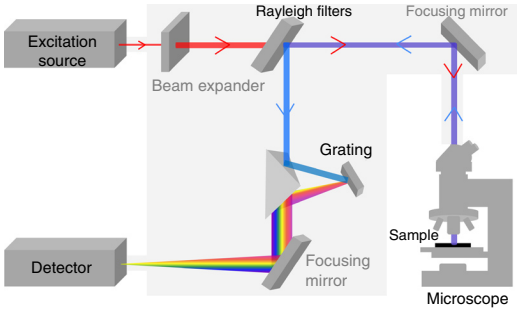

Figure 3 | Generalized overview of instrumentation options within a typical spontaneous Raman spectroscopic microscope system. The beam path will vary slightly between manufacturers, and thus it may contain additional optical components.

what compounds are present in your sample) and diagnostic (where you are using the presence of a compound or a molecular fingerprint to draw conclusions about the sample; see Step 17 of the PROCEDURE). Within these aims, you will have analytical goals or expectations that may be one of the following types: pattern finding, biomarker identification, or spectral classification for diagnostics or imaging[79,87].

Raman microspectroscopy can be used to analyze a wide variety of sample types including fresh plant material (Step 1A), fixed mammalian tissue (Step 1B), biofluids (Step 1C) and cultured mammalian cells (Step 1D). The constraints of the sample under investigation need to be considered (e.g., format, impurities) along with the investigative aims and analytical goals when deciding what equipment to use and how it should be set up. The first decision to make is what excitation source to use.

Excitation source. It is possible to use a variety of excitation sources to irradiate samples, depending on the suitability of the specimen to increased photon energies, as well as on the sensitivity and resolution required in the study. Broadly speaking, there are three main parameters to consider when choosing a laser system: (i) the type of laser source, (ii) the desired wavelength and (iii) the desired spot size.

There are several laser source options available within Raman systems, of which diode lasers are increasingly commonplace, particularly within biological investigations. Diode lasers are based on solid or semiconductor technology, and consequently they provide greater energy efficiency than their popular noble gas–based counterparts[88,89]. Although gas-based lasers have been frequently used in laser-based technologies, they are restricted by a finite lifetime. A helium neon (HeNe) laser has a relatively low power output in comparison with diode lasers, and more powerful alternatives, such as the argon-ion laser, discharge large amounts of heat that require a cooling system to counteract, which is energy inefficient and also reduces portability[88]. The introduction of diode-based lasers has contributed to the development of portable Raman systems because of their durability and compactness[90,91].

When choosing a laser source, it is also important to consider whether the experiment requires the use of pulsed rather than continuous-wave lasers. For example, a pulsed laser would be required in a stimulated Raman spectroscopy system, as the more intense electric field strength of the laser pulse energy can contribute to the increased frequency of Raman scattering events.

The line width of the laser is also an important consideration, as it has a direct influence on the spectral resolution, regardless of spectrometer configuration. Generally, gas-based and solid-state

TABLE 1 | Raman microspectroscopy method derivatives and the respective experimental benefits and limitations.

Technique	Adaption	Benefits	Limitations	Applications/references
Coherent anti-Stokes Raman scattering (CARS)	Nonlinear approach that uses multiple laser frequencies; a pump (ω_p) and Stokes (ω_s) field that combine, tuned to a frequency equivalent to a specific molecular vibration, thus generating a strong anti-Stokes signal ($\omega_{as} = 2\omega_p - \omega_s$) that detects vibrational coherence	10^3–10^6 increased signal[153] High sensitivity 3D imaging	Nonresonant background can dominate weak resonance signals	Cell imaging[154,155] Tissue imaging[156,157] Cancer diagnosis[158,159] Pharmaceuticals[160,161]
Confocal Raman microscopy	Addition of a confocal microscope that allows depth measurements within a tissue. A pinhole is used within the spectrometer to reject stray light, effectively reducing the collimation of the beam and information to be derived from an alternative focal plane	High sensitivity High lateral and depth resolution 3D imaging Rapid acquisition	Diffraction-limited resolution	Cell imaging[162,163] Tissue imaging[164] Cancer diagnosis[165–167] Pharmaceuticals[168,169] Plant cell imaging[74,75]
Drop-coating deposition Raman spectroscopy	Sample preparation for fluid analysis that drops a small volume of sample onto a flat substrate and allows it to dry	Accurate preparation of biofluids Small volumes of fluid are required (2–10 µl)	Not completely free from the 'coffee ring' effect	Biofluid analysis[119] Protein quantification[117,120]

(continued)

TABLE 1 | Raman microspectroscopy method derivatives and the respective experimental benefits and limitations (continued).

Technique	Adaption	Benefits	Limitations	Applications/references
FT-Raman	Nondispersive system that uses FT using a Michelson interferometer	High throughput High resolution Free from fluorescence	Low scattering intensity Limited to IR measurements Detector noise limited	Pharmaceuticals[13,170] Plant materials[71,171]
Kerr-gated Raman spectroscopy	A linear technique that uses repeated laser pulses and a Kerr gate that capture Raman light temporally (up to 3 picoseconds)	Depth measurements up to several millimeters Fluorescence rejection High sensitivity	Not completely free from fluorescence Better performance when in conjunction with shifted excitation Raman difference spectroscopy (SERDS)	Depth profiling in human tissue[172–174]
Polarized Raman spectroscopy (PRS)	Polarized light with a specific electric field vector will only obtain spectral information from specific vibrational modes, depending on their orientation in relation to the incident beam	Information regarding molecular structure and orientation	Not applicable to most samples Loss of spectral information Time consuming	Collagen orientation[175] Plant photosystems[176]
Raman optical activity (ROA)	By using right- and left-circularly polarized incident light, the small changes in Raman scattering can be indicative of optical activity of discrete molecular vibrations	Structural information from specific conformations of chiral molecules	Circular intensity differences are very small Vibrational coupling in ROA signals can prevent accurate band assignment	Biopolymer analysis[177–179] Pharmaceuticals[180,181]
Resonance Raman spectroscopy (RRS)	Exploits the 'resonance effect' observed when the laser frequency matches (or approaches) that of an electronic transition of the sample or compound in question	Up to six orders of magnitude increase in signal[182]	Susceptible to fluorescence interference	Plant photosystems[182] Human biology[54,55,183,184]
SERDS	Nonlinear approach that obtains two spectra at marginally different laser frequencies and creates a difference spectrum by subtracting the two, thus removing background fluorescence	Fluorescence rejection Increased sensitivity	Difference spectra are reconstructed using peak fitting Prone to error	Live cells[185] Animal tissue[186] Human tissue[187]
SORS	Continuous, low-intensity laser beams are used to illuminate the surface of the sample, and Raman spectra are then derived at distinct distances away from this point. A scaled subtraction between these spectra reveals alterations indicative of the underlying subsurface layers	Depth measurements up to several millimeters	Relatively weak signal	Cancer diagnosis[32,188,189] Chemical analysis beneath physical obstructions[190,191]
Surface-enhanced SORS (SESORS)	A combination of SERS and SORS approaches, able to detect SERS nanoparticles introduced into turbid samples	Detects SERS signals up to 50 mm beneath the sample surface[192]	Requires nanoparticle introduction	Depth measurements[193–196]

(continued)

TABLE 1 | Raman microspectroscopy method derivatives and the respective experimental benefits and limitations (continued).

Technique	Adaption	Benefits	Limitations	Applications/references
SRS	Nonlinear approach using a pump (ω_p) and Stokes (ω_s) field that are tuned to a defined frequency representative of molecular vibrations (ω_p–ω_s). When this occurs, ω_p observes a stimulated Raman loss in energy, and ω_s observes a stimulated Raman gain. The transferred intensity is proportional to the biochemical constituents	Not affected by fluorescence and non-resonant background High sensitivity (1 in 10^6 photons) High spatial resolution	Prone to interference from strong Raman scatterers Limited to measurement of one Raman peak per acquisition	Cell imaging[58] Plant imaging[23,197,198]
SERS	Because of surface plasmon resonance, a metal surface with nanoscale roughness can substantially increase the electric field when excited by a laser. Thus, when adsorbed to a biomolecule, these nanoparticles result in greatly enhanced Raman scattering	10^3–10^{10} enhancement Below diffraction limit resolution Quenches fluorescence Low detection limit Molecular labeling	Lack of reproducibility Can reduce band intensity of high-frequency modes Molecular selectivity to nanoparticle adherence	Single-molecule detection[199,200] Tumor targeting[201] Live-cell analysis[202] Pharmaceuticals[203] Cancer diagnosis[62,204,205] Bacterial identification[16,206] Plant materials[207]
Surface-enhanced resonance Raman scattering	Combination of RRS and SERS approaches, using a laser frequency in resonance with a biomolecule of interest and the addition of a SERS active substrate	Up to 10^{15} enhancement[208] Cumulative benefits of both SERS and RRS	Increased experimental complexity	Biomolecule detection[209] Protein analysis[210,211]
TERS	Based on the same electromagnetic and chemical theory as SERS, TERS uses an atomic force microscope tip coated with SERS active metal. When placed in close proximity to the sample, it results in enhanced scattering	Tip-dependent spatial resolution Low detection limit Quenches fluorescence Below diffraction-limit resolution	Increased experimental complexity Sample heating at tip apex	Microbiology[18] Biochemical imaging[212]
Total internal reflection Raman spectroscopy	The sample is placed in contact with a reflective prism, through which a laser beam is reflected, producing an evanescent wave that penetrates the sample below	Defined penetration depth	Reduced surface sensitivity	Plant materials[68]
Transmission Raman	Raman scattered light is captured on the opposite side of laser illumination	Depth measurements up to 30 mm Suitable for opaque materials	Interference from surface molecules	Cancer diagnosis[213] Pharmaceuticals[214,215]

lasers have narrow bandwidths and thus higher spectral resolution, whereas some multimode diode lasers can have wide bandwidths with broad spontaneous emission.

The wavelength of the laser is critical to the experimental design (**Fig. 4**). The wavelengths available are laser-specific, yet they generally fall between the mid-UV (>200 nm) and the NIR (<1.1 µm) regions. Fluorescence contribution (shown in black in **Fig. 4**) to a Raman spectrum can be avoided if you are exciting the sample with a wavelength that falls outside its profile. Therefore, by using NIR wavelengths, the resulting Raman spectrum (shown in red in **Fig. 4**) is free of any fluorescent contribution. Similarly, UV wavelengths can be used, as the fluorescence resulting from light of these wavelengths is red-shifted beyond the fingerprint region of the Raman spectrum; therefore, the spectrum is comparatively free from fluorescence, despite the fact that higher-energy wavelengths are used[76].

Because of the effects of phototoxicity, a key constraint to consider is the interaction between the laser wavelength and the sample. Exposure to high-energy radiation, especially over prolonged periods of exposure, can have a destructive effect on samples. This is particularly important when conducting *in vivo* studies and interrogation of sensitive samples such as single cells.

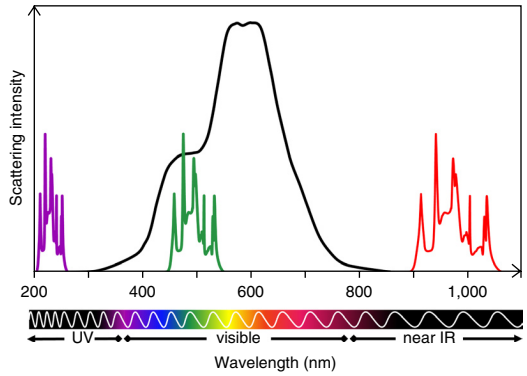

Figure 4 | Simplified overview of the effect of laser excitation wavelength on the fluorescence background. Visible lasers, such as the 532-nm (green) laser, are largely susceptible to background because of the defined wavelength profile of fluorescence (black), whereas high-energy UV (purple) and lower-energy IR (red) wavelengths, such as those at 244 and 1,064 nm, respectively, are relatively free of fluorescence.

Although reducing the laser power at the sample can decrease photodamage and the effects of phototoxicity, not all laser wavelengths are suitable for a given sample, and this should be considered beforehand; for example, cellulose is rapidly damaged at UV wavelengths. It is advised to reduce exposure times wherever possible and to conduct controls to determine the toxic effects of the laser wavelength in use.

In addition, the effect that laser wavelength has on other key experimental parameters such as resolution and sensitivity must also be considered. The spatial resolution is dependent on the spot size of the illuminating beam, which is dependent on the optics and the wavelength of the laser. Sensitivity is also dependent on the excitation wavelength, as the Raman scattering intensity is proportional to $1/\lambda^4$, resulting in substantially reduced sensitivity at lower laser photon energies, such as at the 1,064-nm laser wavelength.

NIR lasers, most commonly those at 785 and 830 nm, have been extensively applied in biological studies, particularly in fixed and live cells, as these lasers have relatively low photon energy and generally do not cause substantial photodamage[92–95]. Tissue Raman microspectroscopy is also typically performed in the NIR region, because it is within the diagnostic window of low melanin and water absorption[96]. For some molecules such as DNA, it makes more sense to perform excitation in the UV region, because the laser frequency and the electronic transition of the molecule under investigation are similar[97,98]. This would provide a molecule-specific enhancement of the scattering, termed resonance Raman scattering.

Practically speaking, it is better to have >30 mW laser power at the source for the shorter visible wavelengths and >100 mW for the longer ones, and then to use a series of attenuators to optimize the illumination power delivered at the specimen. The total laser intensity (power/area) illuminating the sample is a central factor when aiming to acquire high-quality results from biological samples, given that they are generally low-scattering materials that suffer from radiation damage. It is important to consider this last point, as the laser intensity is dependent on laser spot size (sampling area) and magnification; therefore, these factors can have a major impact on the laser exposure of the sample.

It is possible to alter the profile of the laser spot in some Raman systems. By focusing the laser in a line (rather than a spot), a larger surface area is illuminated, which results in more Raman scattered light. Thus, spectral information is obtained from a larger surface area, and photodamage is reduced[99]. Raman maps can be obtained by raster-scanning the line-focused laser across the sample. Line mapping can be achieved in shorter acquisition times compared with point mapping, without compromising image quality[83,100–102]. However, the intensity across the laser line is variable, and therefore this approach leads to spectra with variable signal-to-noise ratios (SNRs) across the laser line, unless corrections are applied to compensate for this. An alternative is to globally illuminate the sample area, often via a fiber-optic array probe, resulting in high-quality spectral imaging with enhanced power distribution across the sample[103,104]. Specialized filters (e.g., liquid-crystal tunable, dielectric acousto-optic filters) are used to actively select specific wavelengths from the sample, which along with a 2D detector allows the production of true Raman images from relatively flat samples[101]. Although global illumination allows for the production of high-quality images, this often comes at a cost of the underlying spectral quality due to the reduced laser intensities across the sampling area.

After considering how best to illuminate the sample, we need to turn our attention to the choice of detector.

Detector. To detect the weak intensity of scattering, the detector included in the Raman system needs to be extremely sensitive. Greater levels of sensitivity may be necessary in some studies in which scattering is especially weak, or in which noise is particularly high, and thus the challenge of detection is increased. Charge-coupled devices (CCDs) are commonly integrated in Raman systems, because they exhibit high quantum efficiencies and low SNRs, compared with early alternative detectors such as photomultiplier tubes (PMTs) and photodiode arrays (PDAs)[105]. CCDs are multichannel arrays made up of thousands of pixels, each of which can collect charge from scattered photons[106]. This charge is directly proportional to the Raman scattering intensity. The CCD detector then reads out this charge by translating it from one pixel to the next until it reaches the edge of the detector chip and can be read out by the readout electronics. There are a range of CCD choices available, including intensified CCDs (ICCDs) and electron-multiplying CCDs (EMCCDs). At extremely low scattering intensities, EMCCDs can provide superior sensitivity than conventional CCDs by creating further electrons and therefore providing a signal relatively higher than the readout noise. However, if spectra are shot noise– or Poisson noise–limited, as is usually the case with biological tissues and cells, the use of an EMCCD will not improve SNRs[107]. Dark, or thermal, noise can be markedly improved by detector cooling, often by using liquid nitrogen cryogenic or thermoelectric Peltier cooling, with deep cooling toward −80 to −100 °C providing up to one order of magnitude improved noise reduction[108].

The quantum efficiency of the silicon-based CCD detectors is wavelength-dependent, and it drops off rapidly in the NIR region. In this spectral region, back-illuminated CCDs could suffer from fringing effects, as the detector thickness effectively behaves as a wavelength resonator. Thus, longer wavelengths of light may not be effectively absorbed and can result in signal modulation and artifacts that could appear in the spectra, with detrimental effects on spectral quality. The use of deep-depletion CCDs can reduce fringing effects, as a thicker photosensitive region is used so that reflection of NIR light is reduced. For NIR studies beyond 950 nm,

in which the photon energy is less than the silicon bandgap, multichannel array detectors such as indium gallium arsenide (InGaAs) detectors are advantageous in order to overcome thermally generated noise in the higher-wavelength region[109].

There are a number of additional hardware options and parameters that can affect experimental output. These include the choice of filters and monochromators, the sampling aperture and the microscope objective.

Filters and monochromators. Rayleigh scattering is more intense than Raman scattering and can easily overpower the more informative signal, so it must be optically filtered. Dispersive Raman spectrometers use specialized Rayleigh filters or a multistage monochromator, whereas nondispersive spectrometers often use Fourier transformation (FT) based on a Michelson interferometer[109]. There are a range of manufacturer-specific Rayleigh filters available[110]; however, holographic notch and dielectric edge filters are most commonly used. Edge filters only transmit light wavelengths above that of the laser in use, whereas notch filters will effectively filter only the laser wavelength, allowing both Stokes and anti-Stokes measurements[111]. Metal oxide edge filters have been shown to have much longer lifetimes than notch filters.

Rayleigh filters must be selected to be specific to the laser wavelength. Multistage monochromators with variable laser wavelengths can be used, but there is a major throughput disadvantage to using multistage monochromators[6]. Single monochromators comprise a diffraction grating, which is used to disperse the Raman scattered light, and they are universally used in conjunction with Rayleigh filters. Gratings differ with respect to the number of grooves (per mm) or lines (per mm) on the surface, which can be anywhere in the range of 150–4,000 per mm, corresponding to the diffraction or angular dispersion capabilities of the grating. Higher groove frequency can improve the spectral resolution at the cost of reduced spectral intensity and range.

Sampling aperture. The sampling aperture of the system determines how much light, and therefore Raman scatter, is passed through the spectrometer. Slits and pinholes range from 10 to 100 μm, with a larger aperture allowing more light through the system and thus increasing sensitivity, but at the expense of spectral and depth resolution. For thin samples such as fixed cells, the use of pinhole and optimal in-depth focus of the laser illumination is crucial to maximizing the Raman signal from the sample volume.

Microscope objective. The choice of microscope objective is crucial in Raman microspectroscopy. The objective's throughput depends on its magnification and solid angle of light collection—i.e., NA. A high-magnification/high-NA objective provides higher axial spatial resolution, but it has a shorter working distance and may be better suited for thin samples. Low-magnification/moderate-NA objectives provide lower axial spatial resolution, but they have a longer working distance and may be better suited for bulky specimens to avoid the specimen touching the objective. Low magnification may be more appropriate for samples that do not require high spatial resolution, such as liquids and homogeneous samples. Conversely, high magnification is beneficial in studies that require high spatial resolution so that specific biological architecture can be examined.

Importantly, microscope objectives can be specially coated in anti-reflective materials or wavelength filter coatings for optimal performance in a specific wavelength region, and those coatings can produce significant background signals if another wavelength is used. We encourage careful consideration of the microscope objective and additional preliminary tests with the sample under investigation.

Experimental design: sample preparation

One of the major advantages of Raman microspectroscopy in biological studies is the ability to derive label-free and nondestructive spectral information with minimal sample preparation. However, it is important to appreciate sample constraints, as well as substrate options, that can have a substantial effect on experimental procedures. Sample stabilization and relative flatness are also important sample preparation considerations, because the technique relies on maintaining optical focus.

Sample format. Although it is possible to analyze fresh tissues directly, fixation can be an important step in preparing mammalian tissue samples or samples of cultured cells. Advantages are that it is a standard method for sample archiving, that it is easy to obtain thin sections from fixed and embedded tissue, and that fixation isolates a sample at a distinct experimental time point.

Formalin-fixed, paraffin-embedded (FFPE) tissues have been historically archived in pathological settings, and these specimens have been widely analyzed using microspectroscopy. A problem for Raman analysis of these samples is that formalin modifies proteins by cross-linking, and it can thus alter spectral peaks associated with proteins between 1,500 and 1,700 cm^{-1}. Furthermore, paraffin has strong signals in the fingerprint and higher-wavenumber regions of the spectrum. These signals can be found at 892, 1,065, 1,135, 1,174, 1,298, 1,421, 1,443 and 1,464 cm^{-1}, and thus they have substantial overlap with the underlying sample biology[112]. The contributions of paraffin in the Raman spectrum can be removed by either de-waxing the sample or by digital de-waxing, which can remove the strong paraffin peaks from the spectrum[113]. De-waxing, as well as the fixation process itself, has been shown to have a marked effect on lipid content in samples, and it should therefore be used cautiously when drawing conclusions based on lipid alterations[114]. Digital de-waxing avoids modifying the sample molecularly, yet it can limit the number of viable spectral regions that can be interpreted. In the PROCEDURE, we describe sample de-waxing using xylene (Step 1A).

Analysis of fresh or snap-frozen tissues may overcome these substantial drawbacks, although sample acquisition becomes more difficult, sectioning is encumbered and sample degradation must be controlled. Live-cell analysis is a rapidly expanding field that allows the user to interrogate cells *in situ* in aqueous environments and 3D cell cultures while maintaining key growth parameters, including temperature and gas availability[56]. In these studies, it is important that the cells adhere sufficiently to a growth substrate before analysis. In addition, the background signal from the cell medium should also be considered beforehand, as it may provide unwanted background interference.

Liquid samples can be easily examined by Raman microspectrometry. This can be achieved using either an immersion

objective or a microfluidic device to overcome spectral artifacts due to the presence of bubbles and surface tension. This has permitted the analysis of biofluids, such as blood plasma, sputum, saliva and urine, in diagnostic studies[51]. Another approach for biofluid analysis is a combined drop coating deposition Raman spectroscopy (DCDRS), which is also known as drop deposition/Raman spectroscopy; this is covered in Step 1C. Small biofluid volumes are deposited onto a flat substrate and allowed to dry on the basis of sessile drop formation principles[115]. Sessile drop formation has many benefits for Raman spectroscopy, with preconcentration of proteins, coarse separation of impurities and reproducible prediction of protein solution concentrations[116,117]. The resultant 'coffee ring' dried drop can be examined by Raman microspectroscopy, with the knowledge that a variable coffee ring thickness affects spectral intensities and the distribution of macromolecules within the ring deposit[118–120].

Raman substrates. Substrate choice is a critical factor in experimental design, and it is dependent on the experimental outputs and sample characteristics. The matrix on which a sample is supported contributes to physical stability, and therefore it directly affects the spectral quality by keeping the sample in focus for the duration of the experiment. The most important properties of the substrate to consider are the spectral background signals, as well as the substrate cost, availability and composition. Care should be taken in choosing a substrate and appropriate preliminary experiments should be performed, because contaminants can produce unwanted background signals. The glass slides typically used in optical microscopy are exceptionally cost effective, but they have a strong background fluorescence at most wavelengths except 532 nm (ref. 121). One approach is to use metal-coated glass slides, such as aluminum- or gold-coated glass, which effectively eliminate the glass signal. Gold-coated slides with roughened surfaces have also been shown to be good SERS substrates[122]. Calcium fluoride (CaF_2), quartz or fused silica slides are used as Raman substrates, because they show minimal background interference. Barium fluoride (BaF_2) slides have also been used as Raman (and IR) substrates, but their partial solubility in water makes them unsuitable for *in vivo* and aqueous studies[123]. Although these specialty substrates are more expensive than glass, they are often reusable in a laboratory setting. In a clinical setting, these costs may be prohibitive, particularly for large-scale screening programs. The development of low-cost, single-use sterilized Raman substrates is an ongoing process in which there have been a number of recent developments, including the use of aluminum foil[124].

SERS. To acquire enhanced spectra using the SERS technique, a greater degree of sample preparation is required than in traditional approaches. As mentioned previously, SERS relies on the interaction of materials with nanoscale roughness with biomolecules within the sample, and the user must first decide on an appropriate SERS substrate. Gold and silver nanoparticles are considered ideal SERS substrates for biological studies using radiation in the visible and NIR regions, as their plasmon resonance frequencies are within this range, although other noble metals such as platinum can be used. The enhancement capabilities of metallic nanoparticle solutions are highly dependent on nanoparticle size, shape and aggregation[125,126]. Theoretically, as nanoparticles increase in size, the resonance will red shift; however, at diameters >100 nm, this comes at a cost of increased resonance linewidth and therefore specificity. Metallic nanospheres have been commonly used in SERS studies, although novel nanostructures such as nanorods and nanostars have exhibited optimized enhancement of the Raman signal[127].

Label-free detection of analytes is a relatively simple SERS approach, which does not require substantial sample preparation. Colloidal nanoparticles can be mixed at a user-defined ratio with other liquids or applied directly onto a sample and allowed to dry. Provided that substantial adsorption occurs between the nanoparticles and the sample, it is possible to acquire consistent, enhanced spectra from homogeneous samples. Conversely, the enhancement effect and resultant spectra become more variable in complex samples, as nonspecific enhancement of each biomolecule within the sample can occur (**Fig. 5**). This issue can be overcome by using SERS labels to specifically target molecules of interest, and it has proven to be a valuable tool in analytical studies[64,65].

Experimental design: spectral acquisition

The desired spectral output must be considered when approaching spectral acquisition, as the experimental parameters for simple point spectra and image construction are different (Steps 7A and 7B). A point-mapping approach allows the user to actively, or randomly, select specific areas of the sample to interrogate with the laser spot. In contrast, an image-mapping approach will derive spectra in a stepwise manner across a larger sample area, thus allowing image generation. In general, superior spectral quality can be obtained using a point-mapping approach, as data sets can benefit from longer acquisition times. In comparison, hyperspectral data cubes generated from mapping and imaging techniques can provide user-friendly data interpretation, although a balance between extensive acquisition times and spectral and image quality is required[101]. For example, a map spanning a biological feature 10 × 10 μm in size would be made up of 100 spectra when using a step size of 1 μm (with oversampling). This map could be acquired

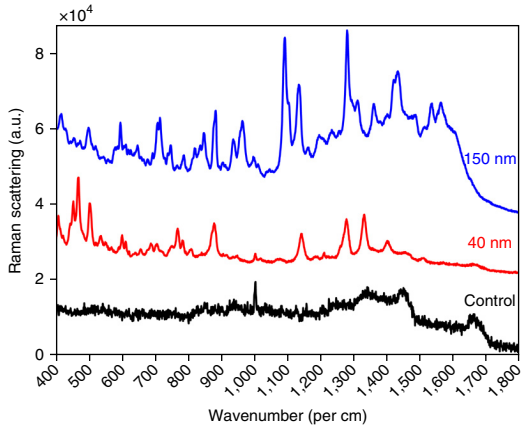

Figure 5 | Raman spectra derived from blood serum containing 150- and 40-nm diameter gold nanospheres, and a control sample containing no SERS substrates. An enhancement effect can be seen in comparison with the control sample, with a 10- and a 30-fold increase in scattering intensity with 40- and 150-nm nanoparticles, respectively (not to scale). However, clear spectral differences are evident because of the complex nature of the sample and the distinctive effects of nanoparticle diameter. a.u., arbitrary units.

relatively quickly when using acquisition times <10 s, although some samples may require longer laser exposures because the sample volume is small or because the sample has weak scattering tendencies (as the latter is relevant for single-cell studies, for example). However, it is important to note that huge numbers of poor-quality spectra can still provide exquisite detail if multivariate approaches are used to analyze the data.

Resolution. The desired spectral and spatial resolution of the experiment, and hence the required sensitivity, must be decided before spectral acquisition. As mentioned with regard to instrumentation options, spatial resolution is ultimately diffraction limited and therefore linearly dependent on the laser wavelength, and it is inversely proportional to the NA of the objective. Accordingly, high spatial resolutions can be achieved with lasers at shorter wavelengths and high-magnification optics.

In contrast, spectral resolution is greater at higher excitation wavelengths, provided that the Raman optical configuration remains constant. An increased number of smaller-sized pixels within the detector and lower levels of cross talk between pixels can also contribute to higher spectral resolution[128]. Spectrometer focal length (SFL) is the distance between the diffraction grating and the detector. This distance is typically 200–800 mm, with greater distances generally providing improved spectral resolution[129]. A larger SFL requires a larger entrance slit, in order to allow the maximum passage of light, which can also influence spectral resolution[130]. However, it is often impractical to alter these parameters within a single Raman system. Gratings with higher groove frequencies can improve spectral resolution at a cost to sensitivity and spectral range, and they can be relatively easy to change on a single Raman instrument.

It is evident that when choosing a laser excitation wavelength there is a potential trade-off between desired spectral and spatial resolution. High spectral resolution (up to 0.5 cm^{-1}) may be required in studies in which specific molecular information is required and thus adjacent Raman bands need to be differentiated, such as in pharmaceutical studies monitoring drug uptake at the cellular level. Increased spatial resolution (up to 1 μm) is required when specific localized information is required, which is particularly important when interrogating tissue features to extract biological information. This is particularly valuable in mapping and imaging approaches, as specific architecture can be imaged, such as when identifying cancer progression in tissue samples[42,45].

Although they are not exhaustive, these factors determine the spectral output and must be considered before analysis. Once these parameters have been chosen, there are steps that can be taken to optimize the experimental conditions. These include instrument calibration (Step 4), adjustment of experimental parameters to optimize for spectral quality and determination of the levels of spectral contamination, which are discussed below.

Calibration. Commercially available instruments produce the Raman spectrum as given wavelengths of light strike the detector at defined pixel values. The process of calibrating the spectrum from pixels to Raman shift, typically reported in wavenumbers, is a multistep process. We recommend daily calibration of the instrument (according to the numbered guidelines below), as even subtle shifts in the instrument optics may produce an observable change in the Raman shift.

(1) It is important that the user ensure that the laser spot corresponds to the visual and spectrometer sampling point before sample acquisition. If necessary, beam alignment can be performed using manual or computerized beam-steers, and it should be checked regularly to optimize spectral acquisition.
(2) Depending on the instrument manufacturer, there are manual and/or automatic calibration options. The first calibration step is conversion of pixels to wavelength. This is achieved by measuring the light emissions of a calibration lamp (such as neon or argon) that has multiple atomic emission lines, and using a nonlinear model to fit the spectral peaks to the CCD pixel.
(3) The second and third steps are converting wavelength to wavenumber units by forming the inverse of the wavelength and correction of the laser wavelength using reference materials with defined Raman signatures. The easiest reference material to use is silicon, which has a sharp peak at 520.5 cm^{-1}, and any band shifts can be easily offset[131]. Other Raman reference materials include cyclohexane, acetaminophen or Teflon. Luminescent or broadband emission standards can be used to derive a system response function measure to correct for filter, detector etaloning and quantum efficiency effects[132]. Further performance validation tests can include the measurement of a well-characterized protein in order to check SNR and calibration consistency between measurements. National Institute of Standards and Technology (NIST) standards are also routinely used as calibration references.

Spectral quality. Optimizing experimental parameters is an iterative process, requiring an element of trial-and-error to obtain a method for optimum spectral quality and high SNR. Spectral quality is governed by instrumentation, sample suitability and, ultimately, time constraints. Within these constraints, the following steps can be followed to improve spectral quality:

(1) Depending on the sample type, it is possible to attenuate the laser power so that higher power is used for weak scatterers to get the highest possible Raman signal, and lower power is used for intense scatterers in order to prevent detector saturation[128].
(2) After power adjustments, the exposure time of the laser on the sample can be increased, thus multiplying the intensity of scattered photons and therefore the spectral quality.
(3) The user also has the option to accumulate multiple spectra, increasing the signal intensity and reducing baseline interference. Longer exposure times and acquiring multiple spectra, commonly referred to as coadditions, can substantially affect sampling times, thus resulting in a potential trade-off between spectral range, quality and time availability.

Spectral contamination. There are a variety of common contaminants that can be observed in Raman spectra, some of which can be sample or instrument dependent. As previously described, fringing effects from the detector and unwanted background from sample substrates are examples of potential spectral contamination. Others include:

(1) Cosmic rays are sporadic background artifacts recognized by sensitive detectors, which manifest in Raman spectra

as narrow-bandwidth spikes[133]. Most of the instrument software packages contain cosmic ray removal algorithms that allow the user to selectively eliminate cosmic rays, as well as algorithms in processing packages for automated cosmic ray removal[134].

(2) Peaks from known contaminants, such as paraffin in FFPE tissues, can be removed using wavenumber exclusion techniques or computational algorithms, which are widely available on instrumentation software, as well as analysis programs[112].

(3) For samples that contain extrinsic fluorescence, photobleaching could be used to suppress interference from contaminants. Exposing samples to the incident light source for a few seconds before acquiring spectra on the detector, effectively 'bleaching' the fluorescent contaminants, has been shown to reduce oscillating baselines[135].

Experimental design: data processing

Spectroscopic studies can rapidly generate large data sets that require computational processing in order to derive biochemical information. Depending on the specific spectral acquisition and experimental objectives, it is possible to extract informative images, spectral biomarkers and patterns, and also to classify samples on the basis of their spectral fingerprint. As a rule, data processing can be divided into three distinct steps: (i) data set pre-processing, (ii) feature extraction and (iii) classification[79]. **Table 2** provides a list of available analysis software. There is also a strong relationship between Raman and IR spectral analysis (for reviews of this technique, see Baker *et al.*[79], Martin *et al.*[87], Lasch[134] and Trevisan *et al.*[136]).

Pre-processing. Immediately after acquiring the spectra, the quality of the spectral data sets should be assessed, and pre-processing should be applied to improve the accuracy of the study by minimizing insignificant variability[134] (Steps 11–16). At this point, spectra should be corrected for cosmic rays, and the quality of the spectra can be visually assessed. There are some circumstances in which visual inspection of spectra shows clear outliers, including substantial spectral contamination, fluorescence or very poor SNR[137]. In those cases, obvious outliers can be removed from the data set. Other spectra that are outliers in

TABLE 2 | Data analysis software for Raman spectral data sets.

Software	Website	License
CytoSpec	http://www.cytospec.com/ftir.php	Commercial
ImageLab	http://www.imagelab.at/en_home.html	Commercial
MATLAB		Commercial
Biodata Toolbox	http://www.mathworks.com/matlabcentral/fileexchange/22068-biodata-toolbox	Open source
Extended Multiplicative Signal Correction (EMSC) Toolbox	http://www.models.life.ku.dk/emsctoolbox	
IRootLab	https://code.google.com/p/irootlab/	Open source
Multivariate Image Analysis (MIA) Toolbox	http://www.eigenvector.com/software/mia_toolbox.htm	Open source
Multivariate Curve Resolution–Alternating Least Squares (MCR-ALS) Toolbox	http://www.cid.csic.es/homes/rtaqam/tmp/WEB_MCR/welcome.htm	Commercial
PLS Toolbox	http://www.eigenvector.com/software/pls_toolbox.htm	Open source
Raman Processing Program	http://cares.wayne.edu/rp/	Commercial Open source
Origin for Spectroscopy	http://www.originlab.com/index.aspx?go=Solutions/Applications/Spectroscopy	Commercial
PeakFit	https://systatsoftware.com/products/peakfit/	Commercial
Python		Open source
PyChem	http://pychem.sourceforge.net/	Open source
PyVib2	http://pyvib2.sourceforge.net/	Open source
R		
HyperSpec	http://hyperspec.r-forge.r-project.org/	Open source
The Unscrambler X	http://www.camo.com/	Commercial

the data set could be identified using a Q-test or another outlier-detecting algorithm; to reduce user bias, this could be done in addition to or even instead of visual inspection. We recommend sagacious and limited removal of spectra from a data set, particularly with respect to hyperspectral images and small data sets.

Raman spectra are particularly prone to noise, and data may require noise reduction to enhance spectral quality. The first approach to improve the quality of the Raman signal would be to alter spectral acquisition settings, such as by using increased integration times and higher laser power. Sample preparation may also be adjusted by preconcentrating or photobleaching the sample. If these approaches are inadequate, then spectra can be computationally manipulated after acquisition to improve the SNR. Principal component analysis (PCA) is a powerful technique in Raman pre-processing that can effectively reduce the spectra into a defined number of principal components (PCs) that account for significant spectral variance[138]. This technique can be used to reconstruct spectra using only significant PCs, thus retaining important spectral data while removing background noise[139]. Other noise-reduction approaches include Savitzky-Golay (SG) smoothing, minimum noise fraction transform and wavelet denoising (WDN) techniques that can filter high-frequency noise[136]. Although smoothing spectra does reduce the apparent noise, we note that these processes also degrade spectral features, and we recommend limited and cautious use of smoothing.

Sample and background fluorescence, as well as thermal fluctuations of the CCD, can markedly affect the spectral baseline, and therefore baseline correction is necessary. Polynomial baseline fitting attempts to estimate the unknown background. This is often dependent on user-defined polynomial points, and it can effectively abolish sloped or oscillatory baselines[140,141]. Care should always be taken with any baseline subtraction routines, as they can introduce unintended artifacts. Alternatively, first- or second-order differentiation, coupled with SG smoothing, can be applied to mathematically remove contributions from scalar offsets or baseline slopes, while simultaneously resolving overlapped peaks[142]. Unlike polynomial fitting, which yields spectra with conventional morphologies, derivative spectra are transformed and do not have a regular Raman appearance.

After baseline correction, spectra may also require normalization to correct for sample and experimental variables, such as thickness and density. Vector normalization and min-max normalization are two popular methods that can be applied to spectra after any baseline correction algorithms without substantially affecting spectral features[134]. Amide I peak normalization is also commonly used in IR and Raman studies[79]. However, this technique is not appropriate after differentiation, because of the shift of the typical amide bands, or for experiments in which you are measuring changes in protein structure, as all values are scaled to 1.

Finally, an optional data reduction step can be included in the pre-processing procedure to optimize statistical analysis. As highlighted previously, large spectral data sets can often present a significant computational burden, because of the many absorbance intensities contained in a single spectrum. By truncating the spectrum to shorter wavenumber ranges, this burden can be reduced, especially if the range focuses on individual Raman peaks[143]. Alternatively, data-reduction algorithms, such as partial least squares (PLS) or PCA, can be used to reduce individual spectra down to a few key factors, and they have been widely implemented as both pre-processing and feature-extraction steps[136].

The selection of pre-processing steps and the order in which they are conducted has been shown to have a major impact on the outcomes of spectral analysis, thus complicating the development of a universal approach[144]. Wherever possible, we advise the use of derivative baseline correction and vector normalization; although this does require high-SNR data, it can be particularly effective in diagnostic studies. In addition, whenever necessary, the use of noise and data reduction tools can be applied.

Feature extraction. In both exploratory and diagnostic studies, it is important to transform individual spectra into appropriate variables that confer biological information. Feature-extraction methods (see Step 17) range from the very simple, such as defining a band area, to considerably more complicated computational functions. Feature extraction can broadly be split into two distinct approaches: feature construction and feature selection. These approaches are comprehensively reviewed by Trevisan *et al.*[136]. Briefly, feature construction can be defined as the creation of new features in a data set that can infer otherwise obscured information: for example, the previously mentioned linear methods PCA and PLS. This can be exceptionally important for diagnostics, biomarker extraction and pattern recognition in otherwise homogeneous data sets, and it has an important role in hyperspectral imaging, as individual pixels can be reduced to single values relating to spectral intensity or variance[79]. Feature selection approaches extrapolate existing features from the data set, such as specific wavenumbers, that can be used to determine spectral biomarkers and/or feed into diagnostic frameworks[145]. Techniques such as genetic algorithm, multivariate curve resolution and successive projection algorithm have proven to be particularly popular as feature-extraction methods, as only informative variables are included in the resultant model[146].

Classification. Classification of samples based on their spectra is often desirable, in both imaging and diagnostic studies, as spectra can be categorized based on prior user input (supervised classification) or spectral variance alone (unsupervised; see Step 17). Unsupervised classification typically relies on a clustering technique, of which hierarchical cluster analysis, *k*-means clustering and fuzzy C-means clustering are three popular options[80]. PCA is another unsupervised approach that is commonly used to extract key variables describing the largest variance within a data set. In imaging studies, this approach requires no prior knowledge of the sample in question, and it produces information-rich pseudo-spectral images that are ideal for exploratory studies[147]. The loadings or spectral features used to calculate the scores or weight images can provide key information on molecular distributions in a sample.

For diagnostic analysis, supervised classification is most commonly used, as the desired outputs are dependent on class labels provided by the user. This could be gold-standard histopathology, cell type or an alternative measure of class. These class assignments are taken into consideration when implementing the classification technique, using a proportion of the data set, referred to as a 'training data set.' A classifier is then able to categorize a separate 'test data set' accordingly. It is a common approach to validate the classification outputs using an independent data set. Linear discriminant classifiers (LDCs), artificial neural networks and support vector machines (SVMs) are particularly common

machine-learning techniques that effectively classify spectral data, although other techniques are available[148]. Semisupervised classification is an alternative option when some, but not all, data classes can be determined[149,150].

Sample size. Classifier performance and validity is highly influenced by sample size, and thus choosing how many samples to use and also how many spectra to acquire is an essential aspect of experimental design. The number of spectra within a data set can easily surpass millions, as a sufficient number of spectra per sample and class type is required to account for the inherent sample intra- and inter-class variability. However, it must be remembered that the number of spectra is not representative of the sample size, and frequently the number of independent samples is much smaller and may, for example, be determined by the overall patient number in a given study. It has been shown that a sample size of 75–100 is sufficient to train a classification model with good precision and validation[151]. Cross-validation may be a suitable solution in smaller data sets, as resampling approaches can repeat or iterate different training and test data sets for a defined number of times, effectively using as much of the data set as possible[136,152]. However, full independent testing of a previously developed classification algorithm is the ideal approach, if the sample numbers permit.

MATERIALS

REAGENTS

! CAUTION We note that most of the listed reagents are chemicals with potential hazards. Users should consult with the chemical's MSDS and the appropriate facility safety guidelines before handling chemicals.

Raman spectra for each reagent used may be provided by the reagent supplier or accessed via a Raman database provided by the instrument manufacturer.

▲ CRITICAL For all materials listed alternative suppliers can be used, unless otherwise stated.

- Sample acquisition: fixed tissue, fresh tissue, cryosectioned tissue, fixed cells, live cells, biofluids and powders from a variety of biological specimens
  ▲ CRITICAL Research carried out with human subjects must be compliant with the Declaration of Helsinki. Research carried out with animals must be approved by the local institutional review board or animal use ethical board. Approvals must be established before the experiment's start.
- Paraffin wax pelletized with added polymers, 57–58 °C (Fisher Scientific, cat. no. 12624077)
- Liquid nitrogen (BOC, CAS no. 7727-37-9)
- Isopentane (Fisher Scientific, cat. no. P/1030/08)
- Virkon disinfectant (Fisher Scientific, cat. no. NC0480633)

Fixative agents

- Formalin, 10% (vol/vol; Sigma-Aldrich, cat. no. HT5011128)
- Glutaraldehyde, 25% (vol/vol; Sigma-Aldrich, cat. no. G5882)
- Ethanol (Fisher Scientific, cat. no. E/0600DF/17)
- Methanol (Fisher Scientific, cat. no. A456-212)
- Acetone (Fisher Scientific, cat. no. A19-1)
- Osmium tetroxide, 2% (wt/vol; Sigma-Aldrich, cat. no. 75633)

SERS nanoparticles

- Gold, 150 nm (1.66×10^9 particles per ml; BBI Solutions, cat. no. EM. GC150)
- Gold, 40 nm (9.00×10^{10} particles per ml; BBI Solutions, cat. no. EM. GC40)
- Silver, 40 nm (2.6×10^9 particles per ml; BBI Solutions, cat. no. EM. SC40)

De-waxing agents

- Xylenes (Sigma-Aldrich, 534056)
- HistoChoice clearing agent (Sigma-Aldrich, cat. no. H2779)

EQUIPMENT

! CAUTION We note that the listed equipment has potential hazards. Users should consult with the equipment instruction manual and the appropriate facility safety guidelines before use.

- Microtome (Thermo Fisher Scientific, cat. no. 902100A)
- Wax dispenser (Electrothermal, cat. no. MH8523B)
- Sectioning bath (Electrothermal, cat. no. MH8517)
- Centrifuge (Thermo Fisher Scientific, cat. no. 75002410)
- Desiccator (Thermo Fisher Scientific, cat. no. 5311-0250)

Substrates

- Glass slides (Fisher Scientific, cat. no. 12657956)
- CaF_2 slides (Crystran, cat. no. CAFP10-10-1)
- Quartz slides (UQG Optics, cat. no. FQM-2521)
- Gold-coated slides (Platypus Technologies, cat. no. AU.0500.ASLI)
- Aluminum-coated slides (EMF, cat. no. AL134)
- Quartz vial (Starna Cells, cat. no. 1-Q-1)

Accessories

- Laser power meter (Coherent, cat. no. 1098293)
- Microtome blades (Leica Biosystems, cat. no. 14035843490)
- Desiccant (Sigma-Aldrich, cat. no. 13767)
- Embedding base molds (Leica Biosystems, cat. no. 38VSP58167)
- Magnets, weights or mounting putty

Electronic equipment

- Raman microspectrometer (**Table 3** illustrates a number of commercially available systems)
- Computer system: a standard computer should be sufficient for basic spectral acquisition and basic data analysis. As computational demand increases in proportion to the complexity of the data processing, it is advised that a system with sufficient RAM access (upwards of 4 GB) and a high-speed processor be used

REAGENT SETUP

Fixatives Fixatives must be diluted to the appropriate concentration using PBS or saline H_2O solution. They can be refrigerated at 4 °C forseveral weeks before use.

SERS nanoparticles Dilute the nanoparticles to an appropriate concentration depending on the experimental parameters. These can be prepared in advance and refrigerated at 4 °C for several weeks before use.

Fixed tissue Generally, tissues are fixed using an appropriate concentration of chemical fixative, followed by alcohol dehydration. Tissues can then either be desiccated and stored at room temperature (20–22 °C) for a number of months or paraffin embedded. An embedding base mold should be filled with molten wax using a wax dispenser. The sample should be carefully placed into the wax at the desired orientation and allowed to cool. FFPE tissue blocks can be stored at room temperature indefinitely.

Fresh tissue *In vitro* studies, such as when tissue has been excised from the independent sample, will be prone to sample degradation, and thus should be analyzed as soon after excision as possible. Refrigeration at 4 °C may be sufficient for 2–3 d of storage. Tissues may be snap-frozen using liquid nitrogen and isopentane for up to 1 year with minimal effect on sample integrity.

Fixed cells Cells can be fixed using appropriate chemical fixative or a preservative buffer, and they can be stored at room temperature for 1 month, or for 3 months at 4 °C. Cells can be gently centrifuged at 1,000*g* for 5 min at room temperature to form a concentrated cell pellet, wherever necessary.

▲ CRITICAL Splitting cells at ~60% confluence greatly diminishes the number of lipid droplets per cell, which can be caused by cell 'stress'.

Live cells Depending on the desired experimental aims, live cells must be kept in optimum living conditions throughout the study, including the maintenance of nutrient requirements via media, as well as temperature, pH, light and gas conditions.

Biofluids Once obtained, biofluids can be stored at −80 °C for several years to prevent degradation. Before sample preparation, biofluids should be thawed at room temperature or by using a water bath at 35–37 °C.

EQUIPMENT SETUP

Software **Table 3** describes the available software options that come standard with each specific commercial instrument. These software options are essential for spectral acquisition, and they may also provide data processing provisions. However, for specialized spectral analysis, we direct the user to **Table 2**, in which alternative software options are listed.

TABLE 3 | Commercially available instruments and corresponding operational software.

Manufacturer	Instruments	Format	Software
BaySpec	Agility	S	Spec 20/20
	RamSpec	S	
	RamSpec-HR	S	
	Nomadic	M	
	MovingLab	MP	
Bruker Optics	SENTERRA	M	OPUS
	RamanScopeIII	M	
	MultiRAM	S	
	RAM II	S	
	BRAVO	SP	
Horiba Scientific	XploRA Series	M	LabSpec 6
	LabRAM HR Evolution	M	
	Triple Raman Spectrometers	S	
	OEM Miniature Raman	SP	
JASCO	NRS-5000 Series Raman	M	Spectra Manager II
	NRS-7000 Series Raman	M	
	RMP-10	SP	
Kaiser Optical Systems	RamanRXN1	M	iC Raman
	Raman WorkStation	M	HoloMap
Ocean Optics	Maya2000 Pro	S	OceanView
	QE Pro	S	
	Ventana Series	S	
Ondax	THz-Raman Spectroscopy Systems	M	NA
	TR-MICRO	M	
Renishaw	InVia confocal Raman microscope	M	WiRE
	RA100 portable Raman analyzer	SP	
SciAps	Inspector300	S	NuSpec
	Inspector500	S	NuSpec Pro
	ReporteR	SP	
Thermo Fisher Scientific	DXR Series	M	ValPro System Qualification
	FirstDefender RM Chemical	SP	
	Identification System	SP	
	FirstDefender RMX Handheld	SP	
	Chemical Identification	SP	
WITec	Alpha300 Series	M	WITec Suite
	apyron∞	SM	

M, microspectrometer; NA, not applicable; P, portable; S, spectrometer.

PROCEDURE

Sample preparation

1| Prepare the samples and mount them onto appropriate Raman substrates according to option A for *in vivo* plant analysis; option B for FFPE tissue samples; option C for SERS biofluid analysis; or option D for analysis of cultured mammalian cells.

(A) Plant tissue ● TIMING 5 min

(i) Remove the plant sample from the plant specimen (e.g., take a leaf or a section of root).

(ii) Place the sample on a suitable Raman substrate (depending on the thickness of the tissue). We typically use gold-coated slides for plant tissues, as they are not adhered to the surface and the substrate can therefore be reused.
▲ **CRITICAL STEP** Leaf tissue in most plant species should be sufficiently thick to avoid background interference from the substrate. However, root tissues, for example, may require a high-quality substrate.

(iii) Secure the sample using a weight, adhesive or magnet if using a magnetic stage accessory.

(B) FFPE tissue ● TIMING 30 min + de-waxing (1.5 h)

(i) Acquire FFPE tissue blocks from a pathology laboratory with appropriate ethical approval.

(ii) Place an FFPE block on a cool (preferably frozen) surface for at least 10 min.
▲ **CRITICAL STEP** Cooling hardens the wax, which therefore facilitates smooth sectioning.

(iii) Position the block in a microtome sample holder, and begin to trim using large sections (up to 25 µm) until the surface on the tissue is exposed.

(iv) Alter the microtome sectioning thickness appropriately, 5–10 µm is common in histopathology, and begin to cut sample ribbons.

(v) Float individual ribbons in a heated sectioning bath at 40–44 °C.
▲ **CRITICAL STEP** Gentle heat will help relax the wax and enable effective mounting. Heat must not surpass 45 °C, as the sample will begin to degenerate as the wax approaches its melting point.

(vi) Carefully mount the samples onto an appropriate Raman substrate, by using the slide to lift the ribbon out of the water. We typically use Raman-grade CaF_2 slides.
▲ **CRITICAL STEP** If the sample requires de-waxing, proceed to Step 1B(vii), if not, proceed to Step 1B(ix).

(vii) Allow the slide to dry for 30 min.
▲ **CRITICAL STEP** The sample must be adequately adhered to the slide surface before de-waxing or the sample can be lost.

(viii) Immerse the tissue in xylene for 5 min. Repeat this step twice to ensure that wax is adequately removed.

(ix) Clear xylene residues using a 15-min 100% ethanol wash, followed by a further 15-min wash with 90% (vol/vol) ethanol and a final wash for 15 min with 70% (vol/vol) ethanol.

(x) Store the samples at room temperature in a dry environment until analysis.
■ **PAUSE POINT** Samples can be stored for up to 1 year without significant degradation.

(C) SERS biofluids ● TIMING 10 min + drying (24 h)

(i) Obtain biofluid specimens with suitable ethical approval.
■ **PAUSE POINT** Samples can be stored at –80 °C for 1–2 years, depending on license constraints.

(ii) Apply 200 µl of biofluids and 200 µl of colloidal nanoparticles onto appropriate Raman substrate (volumes and ratios can be altered depending on the experimental design).
▲ **CRITICAL STEP** The user has three distinct methods for nanoparticle and biofluid mixture: apply the nanoparticle solution to the substrate, allow it to dry and subsequently add the sample; carry out the reverse of the above process, in which the sample is added first followed by the nanoparticles; or combine the two solutions together and apply the mixture onto the substrate.

(iii) Allow the samples to dry before analysis. Larger sample volumes require extended drying times, and thus we recommend overnight drying as a standard for continuity.
▲ **CRITICAL STEP** As water evaporates from the biofluid, biopolymers can concentrate at the extremities of the drop, thus creating a concentration gradient across the sample. This is known as the coffee ring phenomenon, and we advise the user to appreciate this inconsistency across the sample before sample acquisition.

(D) Cells ● TIMING 12 h for cell attachment + 15 min for sample preparation

(i) Seed a known number of cells onto the appropriate Raman substrate in supplemented cell culture medium, under sterile conditions, and incubate them overnight at 37 °C.

(ii) After 12 h or more, allowing for sufficient cellular adhesion to the substrate, remove cells from the incubator and aspirate off the cell culture medium. Wash the samples with warmed sterile PBS. For live-cell imaging, samples can be imaged in this warmed sterile PBS solution or warmed sterile-filtered 0.9% (wt/vol) NaCl saline solution. Proceed to Step 2.
▲ **CRITICAL STEP** Ensure that all reagents are warmed to 37 °C. Warming reagents to 37 °C reduces the shock to the cells and helps maintain overall morphology.

(iii) For cell fixation, immerse the cells in warmed 10% (vol/vol) formalin for 10 min. Wash the cells three times in warmed sterile PBS to remove any trace of the fixative. Samples can be then measured either dry or in sterile-filtered 0.9% (wt/vol) NaCl saline solution.
▲ **CRITICAL STEP** Ensure that all reagents are warmed to 37 °C. Warming to 37 °C reduces the shock to the cells and helps maintain overall morphology.
■ **PAUSE POINT** Fixed cultured cells can be stored for up to 3 months at 4 °C in sterile NaCl saline solution.

Spectral acquisition

2| Switch on the Raman microspectrometer and open the instrument operating software.
▲ **CRITICAL STEP** Carefully read the instrument operating manual and become aware of the operating features, specifications and safety operating procedures.

3| Determine suitable instrumentation options, including laser wavelength, detector type and suitable optics. Please refer to the 'Experimental design: instrument options' section of the INTRODUCTION for further guidance on these options, and set up the microspectrometer accordingly.

4| Calibrate and align the spectrometer using a calibration source. See the 'Experimental design: spectral acquisition' section of the INTRODUCTION for more information on the calibration procedure and the range of sources available.

5| Mount the sample on the microscope stage for spectral acquisition.

6| Use the microscope at the chosen magnification to examine the sample and focus on a feature of interest.
? TROUBLESHOOTING

7| Determine the sampling area using the microscope and operating software using a point-mapping (option A) or image-mapping (option B) approach. Fewer spectra are acquired in point-mapping experiments. This means that spectral quality can, and should, be optimized in order to get meaningful results. In contrast, image mapping can generally acquire a high number of spectra. This means that the researcher has to find a balance between acquisition time and spectral quality (see 'Experimental design' for further guidance). Very long sampling periods may be impractical in terms of sample throughput, and it might be that the sample degrades during the acquisition. This problem can be reduced using multivariate approaches, which can extract much spectral detail from a large number of noisy data.

(A) Point mapping ● TIMING 1–5 min

(i) Selectively, or randomly, choose numerous points in the sampling area to interrogate (anywhere between 5 and 50 spectra would be typical).
▲ **CRITICAL STEP** In SERS studies, enhanced spectra are obtained from molecules in close proximity to nanoparticles. In a point-mapping approach, we advise that the user determine where the nanoparticles have aggregated and choose points from this region.

? TROUBLESHOOTING

(B) Image mapping ● TIMING 1–5 min

(i) Select a mapping area using a 'shape fill' option (usually rectangular filled).
(ii) Determine the number of spectra to be acquired within the mapping area by altering the step size.
▲ **CRITICAL STEP** Be aware of the step size in use (typically ~1 μm), as sizes above this will result in undersampling, and sizes below this will result in oversampling.

8| Input the optimum spectral parameters to ensure the best SNR and spectral quality within an appropriate acquisition time, depending on the sample suitability. Determination of the laser power at the sample using the designated spectral parameters may be conducted using a laser power meter. This is a useful thing to do, so that the precise amount of power applied to the sample can be defined.

9| Acquire the sample measurement (1 s to 5 min per spectrum).
? TROUBLESHOOTING

10| Save the measurements before data processing, and convert them to a universal format if appropriate.
■ **PAUSE POINT** Data sets can be stored until data processing.

Data pre-processing ● TIMING 10–60 min (depending on data set size)

▲ **CRITICAL** Steps 11–16 highlight possible pre-processing steps that can be performed on the spectral data set in an advised order. All these steps are optional and can be applied in multiple combinations with varying effects on visual output. We recommend that the user observe the spectral output at each stage to inspect any adverse effects on the data sets. For further information, we direct the reader to 'Experimental design: data processing' in the INTRODUCTION.

11| Load the data into the selected software (**Table 2**).

12| Screen the data for anomalies and poor-quality spectra using quality tests.

? TROUBLESHOOTING

13| Apply a noise-reduction technique on the data set, such as PCA, to improve SNR.

14| Conduct a baseline correction algorithm to account for fluorescence interference.

15| Perform a data-normalization approach to account for confounding sample variables.

16| If necessary, perform a data-reduction technique such as simple truncation or PCA to reduce the number of variables in the data set.

Data analysis

17| Choose an appropriate data analysis approach that will extract the required information from your point spectra or images, depending on the desired analysis goal. The options described here are exploratory analysis for pattern finding and biomarker extraction (option A), and diagnostic analysis for spectral classification (option B). For more information, please refer to 'Experimental design: data processing' in the INTRODUCTION.

▲ **CRITICAL STEP** All timings are estimated for typical data sets containing anywhere between 500 and 5,000 spectra. Any deviations from this range will alter these estimates accordingly.

(A) Exploratory ● TIMING 15–60 min (depending on the data set size)

(i) Input the pre-processed data set into a feature-extraction algorithm.
▲ **CRITICAL STEP** For imaging, continue to Step 17A(ii); for point spectra, move to Step 17A(iv).
(ii) For image analysis, use feature-extraction outputs to assign a scalar value to each spectrum (such as wavenumber intensities or PC score).
(iii) Use a color gradient or code for scalar values.
(iv) Visualize analysis output for biomarker and pattern extraction.

(B) Diagnostic ● TIMING 1–4 h (depending on the data set size)

▲ **CRITICAL** For supervised classification, the data set must be split into training and test data sets.
(i) Input the pre-processed data set into a feature-extraction algorithm, either construction or selection, in training mode.
(ii) Apply this trained feature-extraction model to a training data set.
(iii) Train a classification algorithm using this training data set.
(iv) Input the test data set into the trained feature-extraction model followed by the trained classification algorithm.
▲ **CRITICAL STEP** Cross-validation is recommended on small sample sizes.
(v) Obtain a class estimation per spectrum.
(vi) For imaging, this class estimation can be assigned a scalar value and visualized using a color code.

(C) Diagnosis (unsupervised) ● TIMING 15–60 min (depending on the data set size)

(i) Use a clustering classification algorithm to categorize spectra on the basis of spectral variance.
(ii) Assign each cluster a numerical value or color for visualization.

? TROUBLESHOOTING

Step 6: maintaining optical focus

It can be difficult to maintain optical focus if the sample is not secured sufficiently, or if the surface is not adequately flat. Good optical focus is essential for obtaining good-quality spectra; this can be ensured by observing the focus on the sample before and after spectral acquisition. To improve stability, bulky samples should be held in place using magnets or weights when possible, or they should be secured with adhesive materials such as tape. A small amount of mounting clay or putty on the underside of hard specimens may help secure them onto a substrate. This should also help flatten some samples, but it may be necessary to physically smooth sample surfaces, such as when analyzing powders. Increased stability stages are

available, and they are recommended in systems using high magnification (100×), as small stage movements can have more significant effects at high magnification.

Step 7A(i): obtaining enhanced spectra

As enhancement depends on direct sampling of an area in close proximity to a nanoparticle, the probability of acquiring enhanced spectra is particularly low. We recommend isolating nanoparticle aggregates, which, unlike monomers, may be visible under magnification. A good knowledge of the sample in question is needed, and we advise carefully studying subtle differences between control and SERS samples. The use of larger nanoparticles (>100 nm) may also aid in nanoparticle aggregate identification[62]. Otherwise, using an automatic mapping procedure may produce enhanced spectra without the need of substantial user input.

Step 9: insufficient spectral quality

As data are obtained, the user should look out for four key indicators of poor spectral quality: (i) low SNR, (ii) fluorescence baseline, (iii) saturation of the CCD and (iv) photoablation. If any of these are seen, troubleshooting intervention is required.

(i) Low SNR—this is indicated by a strong background signal in comparison with Raman peaks, and it is indicative of insufficient Raman signal as a consequence of the sample or the experimental parameters. First, check that the system is appropriately aligned, that the optical focus is optimized and that the laser illuminates the sample. If possible, increase the laser power, followed by the exposure time and then an increased number of coadditions. If this is not possible, consider system alterations, including an alternative laser wavelength or a Raman approach that is better suited to your sample (**Table 1**).

(ii) Fluorescence baseline—a range of fluorescence manifestations can be observed, depending on the excitation wavelength in use, but it is principally indicated by a strong, broad and featureless spectrum, similar to the fluorescence wavelength profile (**Fig. 6a**). Fluorescence is predominantly due to sample characteristics, although it can be influenced by background conditions, such as ambient lighting. We advise using a UV or NIR laser wavelength, or implementing an alternative Raman approach that can overcome fluorescence, such as SERS or SRS. Photobleaching may also reduce fluorescence contributions, with enhanced risk of photoablation.

(iii) Saturation of the CCD—each CCD will have a limit as to how many Raman-scattered photons it can measure. When exceeded, this limit can be observed on the spectrum by a feature such as a flat-line effect (**Fig. 6b**). As saturation is indicative of increased Raman scattering, this issue is usually found in strong-scattering materials, samples of a large volume and in SERS studies. This can be overcome by attenuating the laser power and/or exposure time on the sample. Saturation cannot be corrected in postacquisition processing.

(iv) Photoablation—some samples will be sensitive to high laser powers and can burn once exposed. Sometimes a burned sample will result in a saturated CCD, and some residue may be on the objective. If a burned sample is observed, inspect the microscope objective for residue and check the CCD signal for saturation. When this occurs, it can lead to visible damage of the sample and increased intensity of amorphous carbon peaks. To avoid photodamage, the laser power and exposure times should be decreased accordingly, or a different laser wavelength could be used. If these approaches are inadequate, the laser

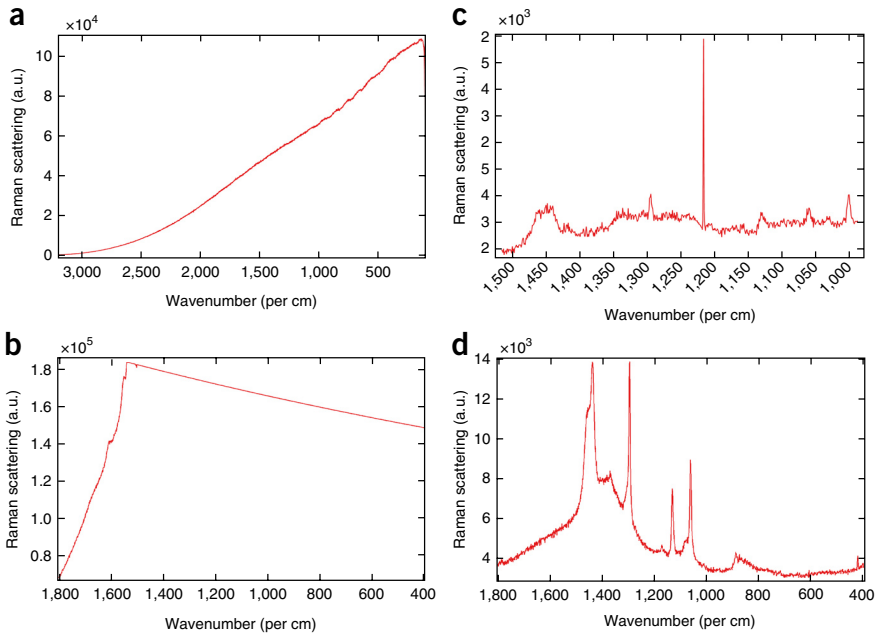

Figure 6 | Examples of common troubleshooting issues during spectral acquisition. (**a**) Typical fluorescence from a urine sample using a 785-nm laser. (**b**) Saturation of a CCD detector from a tomato leaf exposed to excessive laser power. (**c**) Cosmic ray at ~1,220 cm^{-1} from a mapping experiment on endometrial tissue. (**d**) Paraffin contamination from an embedded prostate tissue sample. a.u., arbitrary units.

power can be attenuated at the sample surface by using a larger laser spot, which is achieved by using a lower-magnification setting or altering the laser focus.

Step 12: spectral contaminants

Cosmic rays or interference from sample contaminants can render spectra unusable unless they are removed. Cosmic rays can be identified as sharp spikes with narrow bandwidths that can often overshadow true Raman peaks (**Fig. 6c**). These should be removed using cosmic ray–removal algorithms, which are generally available in instrument operation software. Raman peaks associated with spectral contaminants such as paraffin (**Fig. 6d**) can occur because of inadequate sample preparation; however, these can also be removed with respective computational algorithms, or they can be simply ignored if you are studying spectral regions unaffected by their presence.

● TIMING

We provide approximate times for each of the steps. All timings will depend on the size of the data set, as sample processing and computational analysis are both proportional to the number of samples used.

Step 1A, plant tissue: 5 min

Step 1B, FFPE tissue: 30 min to 2 h

Step 1C, SERS biofluids: 10 min to 24 h

Step 1D, cells: 12 h for cell attachment + 15 min for sample preparation

Steps 2–8, spectral acquisition: 15–25 min

Step 9, point and map acquisition: 1 s to 5 min per spectrum (point mapping: average 15 spectra per sample, ~30 min; image mapping: average 1,000 spectra per sample, ~3 h)

Step 10, saving and converting measurements: 5 min

Steps 11–16, data pre-processing: 10 min to 1 h

Step 17A, exploratory: 15 min to 1 h

Step 17B, diagnostic: 1–4 h

Step 17C, diagnosis: 15 min to 1 h

Minimum experimental time of ~1 h per sample; maximum experimental time of ~32 h per sample

ANTICIPATED RESULTS

Pre-processing options

Figure 7 shows an example of the effects of pre-processing on spectra with strong fluorescence baseline interference (785-nm laser). Spectra were truncated to a defined spectral region (700–1,700 cm^{-1}) to account for Raman peaks present in this particular sample (tomato leaf). A WDN step was performed to smooth the appearance of the data and reduce unwanted noise. With first derivative baseline correction, the SG smoothing function is run simultaneously to account for loss of spectral quality using this approach. This example illustrates how effectively differentiation can account for baseline fluorescence; however, spectral noise is increased and interpretability is reduced because of the transformation of the spectrum. In contrast, polynomial baseline correction results in spectra with conventional appearance and sufficiently relieved of background interference. Vector normalization was used in both

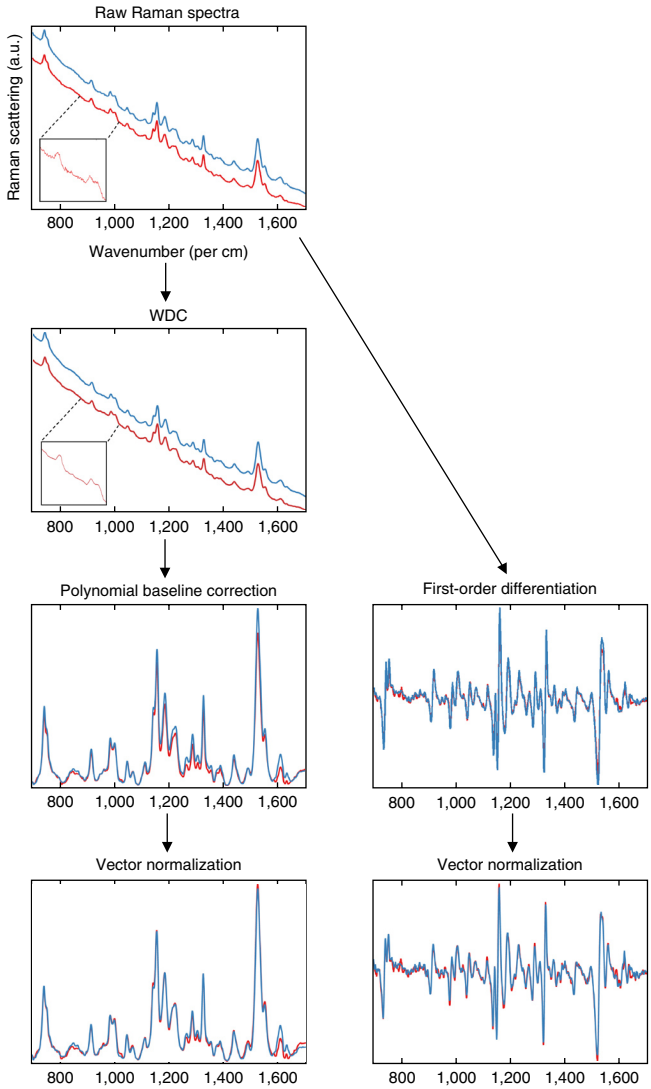

Figure 7 | A brief overview of pre-processing options in Raman spectral data analysis and their contribution to spectral transformation using an example spectrum from a tomato plant leaflet. WDN is conducted as a smoothing process, before polynomial baseline correction and vector normalization. First-order differentiation and Savitzky-Golay smoothing are conducted simultaneously to account for noise introduction in the spectra.

TABLE 4 | Sensitivity and specificity rates (% classification ± s.d.) of control and endometrial cancer patients from blood serum and plasma samples.

		Classification approach (%)			
		SVM		PCA-LDC	
Sample	Pre-processing	Sensitivity	Specificity	Sensitivity	Specificity
Serum	Polynomial→ vector normalization	87.38 ± 8.64	91.78 ± 05.71	84.46 ± 15.38	92.66 ± 07.32
	First-order differentiation→ vector normalization	77.89 ± 06.07	81.37 ± 12.39	80.36 ± 13.41	79.21 ± 09.51
Plasma	Polynomial→ vector normalization	97.8 ± 03.23	96.75 ± 04.50	91.77 ± 09.77	95.33 ± 6.59
	First-order differentiation→ vector normalization	98.42 ± 11.89	98.57 ± 03.19	92.90 ± 05.39	97.24 ± 04.91

Two pre-processing approaches and two classification approaches are used to illustrate varied performances. Polynomial baseline correction was conducted with a polynomial order of five and first-order SG differentiation used nine filter coefficients with a polynomial order of two. A SVM (optimized C and γ parameters) classifier was implemented without a feature extraction step, whereas PCA (optimized number of PCs) was used before a LDC.

incidences to attribute for confounding sample features, such as thickness; the effect of this is a slight reduction in variance between classes.

Classification of blood plasma and serum using SERS

Table 4 illustrates the effect of pre-processing, feature-extraction and classification approaches on blood plasma and serum in endometrial cancer patients[62]. From this study, plasma samples produced better classification rates compared with blood serum; this might be explained by the inclusion of clotting proteins in blood serum. The effect of pre-processing can be seen when comparing the classification rates in serum and plasma, with the former performing better with polynomial baseline correction and the latter performing best with differentiation correction. In this example, the classification approach used had a small effect on rates of classification, but this may not be the case in other circumstances. To assess diagnostic efficiency, a variety of pre-processing and classification approaches should be used and compared.

Mapping of endometrial tissue

Figure 8 depicts FFPE endometrial tissue in control patients in order to identify the epithelial lining of the endometrial crypts. These tissue structures seen throughout the three examples are found ubiquitously throughout endometrial tissue initiating at the lumen and spiraling toward the myometrium (not visible). Each map was acquired using an increasing exposure time (**Fig. 8a–c**), ultimately increasing the spectral quality at each pixel. The Raman data were analyzed using the multivariate technique PCA, with PC2 effectively identifying the connective tissue (red) largely due to protein alterations at 1,003 and 1,280 cm^{-1}, and PC3 depicting the epithelial layer (yellow) surrounding the crypt lumen, due to fatty acid and lipid differences at 1,060, 1,131 and 1,295 cm^{-1}. This was apparent across all three image maps, despite the range of laser exposure times used.

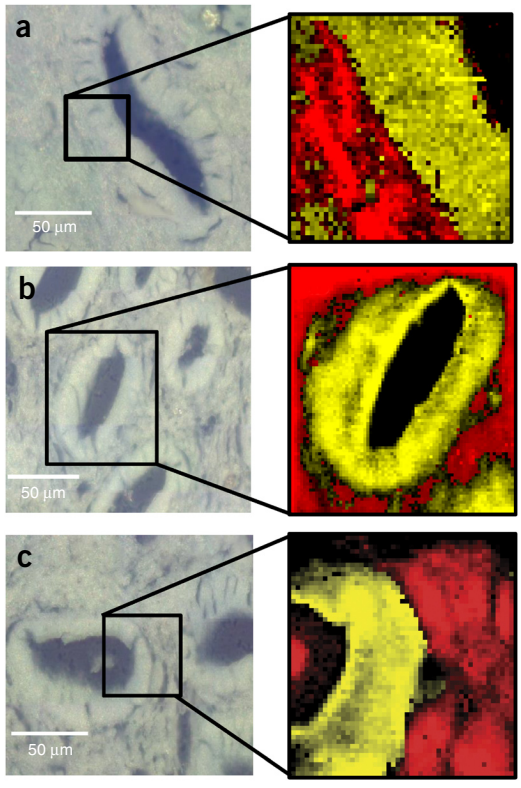

Figure 8 | Raman map of fixed endometrial tissue, focusing on uterine glands that spiral throughout the tissue. Samples are FFPE and were mounted on BaF_2 slides before de-waxing. (**a–c**) Left images are white-light images of the tissues, whereas right images show PCA maps. Epithelial tissue is depicted in yellow, whereas connective tissue is shown in red; these correspond to PC3 and PC2, respectively. Spectra were all obtained using a 785-nm laser with 25 mW of power at the sample, a 1,200 l/mm grating and a step size of 1 μm. Image acquisition parameters were as follows: 5-s exposure time, comprising 47 × 48 pixels (**a**, right); 10 s, with 74 × 81 pixels (**b**, right); and 15 s, with 55 × 53 pixels (**c**, right).

ACKNOWLEDGMENTS H.J.B.'s project is mediated by the Centre for Global Eco-Innovation funding through the European Regional Development Fund (ERDF). Work in F.L.M.'s laboratories has been funded by the UK Engineering and Physical Sciences Research Council (EPSRC), the Rosemere Cancer Foundation and the UK Biotechnology and Biological Sciences Research Council (BBSRC). K.E.-W. acknowledges a Pilot and Feasibility grant from the Michigan Diabetes Research and Training (subsidiary of National Institutes of Health (NIH)/National Institute of Diabetes and Digestive and Kidney Diseases (NIDDK) 2P30 DK020572).

AUTHOR CONTRIBUTIONS F.L.M. is the principal investigator who conceived the idea for and finalized the manuscript; H.J.B. wrote and compiled the manuscript and figures. L.A., B.B., G.C., K.E.-W., B.G., M.J.W., M.R.M. and N.S. provided information and feedback throughout the article; and K.C., J.D., N.J.F. and P.L.M.-H. provided feedback on the manuscript.

COMPETING FINANCIAL INTERESTS The authors declare no competing financial interests.

1. Clemens, G., Hands, J.R., Dorling, K.M. & Baker, M.J. Vibrational spectroscopic methods for cytology and cellular research. *Analyst* **139**, 4411–4444 (2014).
2. Ellis, D.I., Cowcher, D.P., Ashton, L., O'Hagan, S. & Goodacre, R. Illuminating disease and enlightening biomedicine: Raman spectroscopy as a diagnostic tool. *Analyst* **138**, 3871–3884 (2013).
3. Downes, A. & Elfick, A. Raman spectroscopy and related techniques in biomedicine. *Sensors* **10**, 1871–1889 (2010).
4. Krafft, C. & Popp, J. The many facets of Raman spectroscopy for biomedical analysis. *Anal. Bioanal. Chem.* **407**, 699–717 (2015).
5. Movasaghi, Z., Rehman, S. & Rehman, I.U. Raman spectroscopy of biological tissues. *Appl. Spectrosc. Rev.* **42**, 493–541 (2007).
6. Chase, B. A new generation of Raman instrumentation. *Appl. Spectrosc.* **48**, 14–19 (1994).
7. Zhang, Y., Hong, H. & Cai, W. Imaging with Raman spectroscopy. *Curr. Pharm. Biotechnol.* **11**, 654–661 (2010).
8. Kneipp, K., Kneipp, H., Itzkan, I., Dasari, R.R. & Feld, M.S. Surface-enhanced Raman scattering and biophysics. *J. Phys. Condens. Matter* **14**, R597–R624 (2002).
9. Hartschuh, A., Sánchez, E.J., Xie, X.S. & Novotny, L. High-resolution near-field Raman microscopy of single-walled carbon nanotubes. *Phys. Rev. Lett.* **90**, 095503 (2003).
10. Cooper, J.B. Chemometric analysis of Raman spectroscopic data for process control applications. *Chemometr. Intell. Lab. Syst.* **46**, 231–247 (1999).
11. Widjaja, E., Zheng, W. & Huang, Z. Classification of colonic tissues using near-infrared Raman spectroscopy and support vector machines. *Int. J. Oncol.* **32**, 653–662 (2008).
12. Krafft, C., Steiner, G., Beleites, C. & Salzer, R. Disease recognition by infrared and Raman spectroscopy. *J. Biophotonics* **2**, 13–28 (2009).
13. Vankeirsbilck, T. *et al.* Applications of Raman spectroscopy in pharmaceutical analysis. *Trends Analyt. Chem.* **21**, 869–877 (2002).
14. Ekins, S. & Sasic, S. *Pharmaceutical Applications of Raman Spectroscopy* (John Wiley & Sons, 2008).
15. Frosch, T., Yan, D. & Popp, J. Ultrasensitive fiber enhanced UV resonance Raman sensing of drugs. *Anal. Chem.* **85**, 6264–6271 (2013).
16. Jarvis, R.M. & Goodacre, R. Discrimination of bacteria using surface-enhanced Raman spectroscopy. *Anal. Chem.* **76**, 40–47 (2004).
17. Maquelin, K. *et al.* Identification of medically relevant microorganisms by vibrational spectroscopy. *J. Microbiol. Methods* **51**, 255–271 (2002).
18. Neugebauer, U. *et al.* On the way to nanometer-sized information of the bacterial surface by tip-enhanced Raman spectroscopy. *Chemphyschem* **7**, 1428–1430 (2006).
19. Pahlow, S., Meisel, S., Cialla-May, D., Weber, K. & Röschac, J.P.P. Isolation and identification of bacteria by means of Raman spectroscopy. *Adv. Drug Deliv. Rev.* **89**, 105–120 (2015).
20. Ashton, L., Lau, K., Winder, C.L. & Goodacre, R. Raman spectroscopy: lighting up the future of microbial identification. *Future Microbiol.* **6**, 991–997 (2011).
21. Owen, C.A. *et al. In vitro* toxicology evaluation of pharmaceuticals using Raman micro-spectroscopy. *J. Cell. Biochem.* **99**, 178–186 (2006).
22. Knief, P. *et al.* Raman spectroscopy—a potential platform for the rapid measurement of carbon nanotube-induced cytotoxicity. *Analyst* **134**, 1182–1191 (2009).
23. Mansfield, J.C. *et al.* Label-free chemically specific imaging *in planta* with stimulated Raman scattering microscopy. *Anal. Chem.* **85**, 5055–5063 (2013).
24. Baranska, M., Roman, M., Schulz, H. & Baranski, R. Recent advances in Raman analysis of plants: alkaloids, carotenoids, and polyacetylenes. *Curr. Anal. Chem.* **9**, 108–127 (2013).
25. Gierlinger, N. & Schwanninger, M. The potential of Raman microscopy and Raman imaging in plant research. *Spectroscopy* **21**, 69–89 (2007).
26. Kallaway, C. *et al.* Advances in the clinical application of Raman spectroscopy for cancer diagnostics. *Photodiagnosis Photodyn. Ther.* **10**, 207–219 (2013).
27. Byrne, H.J. *et al.* Spectropathology for the next generation: Quo vadis? *Analyst* **140**, 2066–2073 (2015).
28. Meyer, T. *et al.* Nonlinear microscopy, infrared, and Raman microspectroscopy for brain tumor analysis. *J. Biomed. Opt.* **16**, 021113 (2011).
29. Fullwood, L.M. *et al.* Investigating the use of Raman and immersion Raman spectroscopy for spectral histopathology of metastatic brain cancer and primary sites of origin. *Anal. Methods* **6**, 3948–3961 (2014).
30. Gajjar, K. *et al.* Diagnostic segregation of human brain tumours using Fourier-transform infrared and/or Raman spectroscopy coupled with discriminant analysis. *Anal. Methods* **5**, 89–102 (2013).
31. Krafft, C., Neudert, L., Simat, T. & Salzer, R. Near-infrared Raman spectra of human brain lipids. *Spectrochim. Acta A Mol. Biomol. Spectrosc.* **61**, 1529–1535 (2005).
32. Stone, N., Baker, R., Rogers, K., Parker, A.W. & Matousek, P. Subsurface probing of calcifications with spatially offset Raman spectroscopy (SORS): future possibilities for the diagnosis of breast cancer. *Analyst* **132**, 899–905 (2007).
33. Crow, P., Uff, J., Farmer, J., Wright, M. & Stone, N. The use of Raman spectroscopy to identify and characterize transitional cell carcinoma *in vitro*. *BJU Int.* **93**, 1232–1236 (2004).
34. Lin, D. *et al.* Colorectal cancer detection by gold nanoparticle based surface-enhanced Raman spectroscopy of blood serum and statistical analysis. *Opt. Express* **19**, 13565–13577 (2011).
35. Dekker, E. & Fockens, P. Advances in colonic imaging: new endoscopic imaging methods. *Eur. J. Gastroenterol. Hepatol.* **17**, 803–808 (2005).
36. Stone, N., Stavroulaki, P., Kendall, C., Birchall, M. & Barr, H. Raman spectroscopy for early detection of laryngeal malignancy: preliminary results. *Laryngoscope* **110**, 1756–1763 (2000).
37. Huang, Z. *et al.* Near-infrared Raman spectroscopy for optical diagnosis of lung cancer. *Int. J. Cancer* **107**, 1047–1052 (2003).
38. Horsnell, J.D. *et al.* Raman spectroscopy—a potential new method for the intra-operative assessment of axillary lymph nodes. *Surgeon* **10**, 123–127 (2012).
39. Lloyd, G.R. *et al.* Discrimination between benign, primary and secondary malignancies in lymph nodes from the head and neck utilising Raman spectroscopy and multivariate analysis. *Analyst* **138**, 3900–3908 (2013).
40. Stone, N., Kendall, C., Shepherd, N., Crow, P. & Barr, H. Near-infrared Raman spectroscopy for the classification of epithelial pre-cancers and cancers. *J. Raman Spectrosc.* **33**, 564–573 (2002).
41. Kendall, C. *et al.* Raman spectroscopy, a potential tool for the objective identification and classification of neoplasia in Barrett's oesophagus. *J. Pathol.* **200**, 602–609 (2003).
42. Bergholt, M.S. *et al. In vivo* diagnosis of esophageal cancer using image-guided Raman endoscopy and biomolecular modeling. *Technol. Cancer Res. Treat.* **10**, 103–112 (2011).
43. Crow, P. *et al.* Assessment of fiberoptic near-infrared Raman spectroscopy for diagnosis of bladder and prostate cancer. *Urology* **65**, 1126–1130 (2005).
44. Patel, I.I. & Martin, F.L. Discrimination of zone-specific spectral signatures in normal human prostate using Raman spectroscopy. *Analyst* **135**, 3060–3069 (2010).
45. Patel, I.I. *et al.* Segregation of human prostate tissues classified high-risk (UK) versus low-risk (India) for adenocarcinoma using Fourier-transform infrared or Raman microspectroscopy coupled with discriminant analysis. *Anal. Bioanal. Chem.* **401**, 969–982 (2011).
46. Crow, P. *et al.* The use of Raman spectroscopy to identify and grade prostatic adenocarcinoma *in vitro*. *Br. J. Cancer* **89**, 106–108 (2003).
47. Rashid, N. *et al.* Raman microspectroscopy for the early detection of pre-malignant changes in cervical tissue. *Exp. Mol. Pathol.* **97**, 554–564 (2014).
48. Patel, I.I. *et al.* High contrast images of uterine tissue derived using Raman microspectroscopy with the empty modelling approach of multivariate curve resolution-alternating least squares. *Analyst* **136**, 4950–4959 (2011).
49. Krishna, C.M. *et al.* Raman spectroscopy studies for diagnosis of cancers in human uterine cervix. *Vib. Spectrosc.* **41**, 136–141 (2006).
50. Lyng, F.M. *et al.* Vibrational spectroscopy for cervical cancer pathology, from biochemical analysis to diagnostic tool. *Exp. Mol. Pathol.* **82**, 121–129 (2007).
51. Mitchell, A.L., Gajjar, K.B., Theophilou, G., Martin, F.L. & Martin-Hirsch, P.L. Vibrational spectroscopy of biofluids for disease screening or diagnosis: translation from the laboratory to a clinical setting. *J. Biophotonics* **7**, 153–165 (2014).

52. Wood, B.R. *et al.* Raman imaging of hemozoin within the food vacuole of *Plasmodium falciparum* trophozoites. *FEBS Lett.* **554**, 247–252 (2003).
53. Wood, B.R. *et al.* Tip-enhanced Raman scattering (TERS) from hemozoin crystals within a sectioned erythrocyte. *Nano Lett.* **11**, 1868–1873 (2011).
54. Wood, B.R. & McNaughton, D. Resonance Raman spectroscopy in malaria research. *Expert Rev. Proteomics* **3**, 525–544 (2006).
55. Wood, B.R. *et al.* Resonance Raman spectroscopy reveals new insight into the electronic structure of β-hematin and malaria pigment. *J. Am. Chem. Soc.* **126**, 9233–9239 (2004).
56. Bonnier, F. *et al.* Imaging live cells grown on a three dimensional collagen matrix using Raman microspectroscopy. *Analyst* **135**, 3169–3177 (2010).
57. Notingher, I. & Hench, L.L. Raman microspectroscopy: a noninvasive tool for studies of individual living cells *in vitro*. *Expert Rev. Med. Devices* **3**, 215–234 (2006).
58. Zhang, X. *et al.* Label-free live-cell imaging of nucleic acids using stimulated Raman scattering microscopy. *Chemphyschem* **13**, 1054–1059 (2012).
59. Kneipp, J., Kneipp, H., Rajadurai, A., Redmond, R.W. & Kneipp, K. Optical probing and imaging of live cells using SERS labels. *J. Raman Spectrosc.* **40**, 1–5 (2009).
60. Farhane, Z., Bonnier, F., Casey, A. & Byrne, H. Raman micro spectroscopy for *in vitro* drug screening: subcellular localisation and interactions of doxorubicin. *Analyst* **140**, 4212–4223 (2015).
61. Meister, K. *et al.* Label-free imaging of metal–carbonyl complexes in live cells by Raman microspectroscopy. *Angew. Chem. Int. Ed.* **49**, 3310–3312 (2010).
62. Butler, H.J. *et al.* Gold nanoparticles as a substrate in bio-analytical near-infrared surface-enhanced Raman spectroscopy. *Analyst* **140**, 3090–3097 (2015).
63. Ackermann, K.R., Henkel, T. & Popp, J. Quantitative online detection of low-concentrated drugs via a SERS microfluidic system. *Chemphyschem* **8**, 2665–2670 (2007).
64. Harper, M.M., Dougan, J.A., Shand, N.C., Graham, D. & Faulds, K. Detection of SERS active labelled DNA based on surface affinity to silver nanoparticles. *Analyst* **137**, 2063–2068 (2012).
65. Barrett, L., Dougan, J.A., Faulds, K. & Graham, D. Stable dye-labelled oligonucleotide-nanoparticle conjugates for nucleic acid detection. *Nanoscale* **3**, 3221–3227 (2011).
66. Faulds, K., Smith, W., Graham, D. & Lacey, R. Assessment of silver and gold substrates for the detection of amphetamine sulfate by surface enhanced Raman scattering (SERS). *Analyst* **127**, 282–286 (2002).
67. Gill, D., Kilponen, R. & Rimai, L. Resonance Raman scattering of laser radiation by vibrational modes of carotenoid pigment molecules in intact plant tissues. *Nature* **227**, 743–744 (1970).
68. Greene, P.R. & Bain, C.D. Total internal reflection Raman spectroscopy of barley leaf epicuticular waxes *in vivo*. *Colloids Surf. B Biointerfaces* **45**, 174–180 (2005).
69. Schulz, H. & Baranska, M. Identification and quantification of valuable plant substances by IR and Raman spectroscopy. *Vib. Spectrosc.* **43**, 13–25 (2007).
70. Sene, C., McCann, M.C., Wilson, R.H. & Grinter, R. Fourier-transform Raman and Fourier-transform infrared spectroscopy (an investigation of five higher plant cell walls and their components). *Plant Physiol.* **106**, 1623–1631 (1994).
71. Schulz, H., Baranska, M. & Baranski, R. Potential of NIR-FT-Raman spectroscopy in natural carotenoid analysis. *Biopolymers* **77**, 212–221 (2005).
72. Rösch, P., Popp, J. & Kiefer, W. Raman and surface enhanced Raman spectroscopic investigation on *Lamiaceae* plants. *J. Mol. Struct.* 480–481, 121–124 (1999).
73. Schmidt, M. *et al.* Raman imaging of cell wall polymers in *Arabidopsis thaliana*. *Biochem. Biophys. Res. Commun.* **395**, 521–523 (2010).
74. Gierlinger, N. & Schwanninger, M. Chemical imaging of poplar wood cell walls by confocal Raman microscopy. *Plant Physiol.* **140**, 1246–1254 (2006).
75. Gierlinger, N., Keplinger, T. & Harrington, M. Imaging of plant cell walls by confocal Raman microscopy. *Nat. Protoc.* **7**, 1694–1708 (2012).
76. Asher, S.A. & Johnson, C.R. Raman spectroscopy of a coal liquid shows that fluorescence interference is minimized with ultraviolet excitation. *Science* **225**, 311–313 (1984).
77. Butler, H.J., McAinsh, M.R., Adams, S. & Martin, F.L. Application of vibrational spectroscopy techniques to non-destructively monitor plant health and development. *Anal. Methods* **7**, 4059–4070 (2015).
78. Baranski, R., Baranska, M. & Schulz, H. Changes in carotenoid content and distribution in living plant tissue can be observed and mapped *in situ* using NIR-FT-Raman spectroscopy. *Planta* **222**, 448–457 (2005).
79. Baker, M.J. *et al.* Using Fourier transform IR spectroscopy to analyze biological materials. *Nat. Protoc.* **9**, 1771–1791 (2014).
80. Diem, M., Romeo, M., Boydston-White, S., Miljkovi, M. & Matthäus, C. A decade of vibrational micro-spectroscopy of human cells and tissue (1994–2004). *Analyst* **129**, 880–885 (2004).
81. Dumas, P., Sockalingum, G.D. & Sule-Suso, J. Adding synchrotron radiation to infrared microspectroscopy: what's new in biomedical applications? *Trends Biotechnol.* **25**, 40–44 (2007).
82. Bhargava, R. Infrared spectroscopic imaging: the next generation. *Appl. Spectrosc.* **66**, 1091–1120 (2012).
83. Palonpon, A.F. *et al.* Raman and SERS microscopy for molecular imaging of live cells. *Nat. Protoc.* **8**, 677–692 (2013).
84. Felten, J. *et al.* Vibrational spectroscopic image analysis of biological material using multivariate curve resolution–alternating least squares (MCR-ALS). *Nat. Protoc.* **10**, 217–240 (2015).
85. Kong, L. *et al.* Characterization of bacterial spore germination using phase-contrast and fluorescence microscopy, Raman spectroscopy and optical tweezers. *Nat. Protoc.* **6**, 625–639 (2011).
86. Li, J.F. *et al.* Surface analysis using shell-isolated nanoparticle-enhanced Raman spectroscopy. *Nat. Protoc.* **8**, 52–65 (2013).
87. Martin, F.L. *et al.* Distinguishing cell types or populations based on the computational analysis of their infrared spectra. *Nat. Protoc.* **5**, 1748–1760 (2010).
88. Angel, S., Carrabba, M. & Cooney, T. The utilization of diode lasers for Raman spectroscopy. *Spectrochim. Acta A Mol. Biomol. Spectrosc.* **51**, 1779–1799 (1995).
89. Müller, A. *et al.* Diode laser based light sources for biomedical applications. *Laser Photonics Rev.* **7**, 605–627 (2013).
90. Yan, F. & Vo-Dinh, T. Surface-enhanced Raman scattering detection of chemical and biological agents using a portable Raman integrated tunable sensor. *Sensor. Actuat. B Chem.* **121**, 61–66 (2007).
91. Moore, D. & Scharff, R.J. Portable Raman explosives detection. *Anal. Bioanal. Chem.* **393**, 1571–1578 (2009).
92. Draux, F. *et al.* Raman spectral imaging of single living cancer cells: a preliminary study. *Analyst* **134**, 542–548 (2009).
93. Creely, C., Volpe, G., Singh, G., Soler, M. & Petrov, D. Raman imaging of floating cells. *Opt. Express* **13**, 6105–6110 (2005).
94. Swain, R. & Stevens, M. Raman microspectroscopy for non-invasive biochemical analysis of single cells. *Biochem. Soc. Trans.* **35**, 544–549 (2007).
95. Zoladek, A., Pascut, F.C., Patel, P. & Notingher, I. Non-invasive time-course imaging of apoptotic cells by confocal Raman micro-spectroscopy. *J. Raman Spectrosc.* **42**, 251–258 (2011).
96. Vo-Dinh, T. *Biomedical Photonics Handbook: Biomedical Diagnostics* Vol. 2 (CRC press, 2014).
97. Asher, S.A., Ludwig, M. & Johnson, C.R. UV resonance Raman excitation profiles of the aromatic amino acids. *J. Am. Chem. Soc.* **108**, 3186–3197 (1986).
98. Kumamoto, Y., Taguchi, A., Smith, N.I. & Kawata, S. Deep ultraviolet resonant Raman imaging of a cell. *J. Biomed. Opt.* **17**, 076001 (2012).
99. Ivanda, M. & Furić̨ K. Line focusing in micro-Raman spectroscopy. *Appl. Opt.* **31**, 6371–6375 (1992).
100. Okada, M. *et al.* Label-free Raman observation of cytochrome *c* dynamics during apoptosis. *Proc. Natl. Acad. Sci. USA* **109**, 28–32 (2012).
101. Schlücker, S., Schaeberle, M.D., Huffman, S.W. & Levin, I.W. Raman microspectroscopy: a comparison of point, line, and wide-field imaging methodologies. *Anal. Chem.* **75**, 4312–4318 (2003).
102. Minamikawa, T. *et al.* Label-free detection of peripheral nerve tissues against adjacent tissues by spontaneous Raman microspectroscopy. *Histochem. Cell Biol.* **139**, 181–193 (2013).
103. Markwort, L., Kip, B., Da Silva, E. & Roussel, B. Raman imaging of heterogeneous polymers: a comparison of global versus point illumination. *Appl. Spectrosc.* **49**, 1411–1430 (1995).
104. Ma, J. & Ben-Amotz, D. Rapid micro-Raman imaging using fiber-bundle image compression. *Appl. Spectrosc.* **51**, 1845–1848 (1997).
105. Cooper, J. *et al.* Raman spectroscopy with a low-cost imaging CCD array. *Spectrochim. Acta A Mol. Spectrosc.* **50**, 567–575 (1994).
106. LaPlant, F. in *Emerging Raman Applications and Techniques in Biomedical and Pharmaceutical Fields* Vol. 1 (eds. Matousek, P. & Morris, M.D.) 1–24 (Springer, 2010).
107. Dieing, T. & Hollricher, O. High-resolution, high-speed confocal Raman imaging. *Vib. Spectrosc.* **48**, 22–27 (2008).
108. Harnly, J.M. & Fields, R.E. Solid-state array detectors for analytical spectrometry. *Appl. Spectrosc.* **51**, 334A (1997).
109. Li, Z., Deen, M.J., Kumar, S. & Selvaganapathy, P.R. Raman spectroscopy for in-line water quality monitoring—instrumentation and potential. *Sensors* **14**, 17275–17303 (2014).
110. Carriere, J.T. & Havermeyer, F. Ultra-low-frequency Stokes and anti-Stokes Raman spectroscopy at 785 nm with volume holographic grating filters. *SPIE BiOS Proceedings* (Biomedical Vibrational Spectroscopy V: Advances in Research and Industry, January 21, 2012, San Francisco) **8219**, 821905 (2012).

111. Pitt, G.D. *et al.* Engineering aspects and applications of the new Raman instrumentation. *IEE Proceedings: Science, Measurement and Technology* **152**, 241–318 (2005).
112. Tfayli, A. *et al.* Digital dewaxing of Raman signals: discrimination between nevi and melanoma spectra obtained from paraffin-embedded skin biopsies. *Appl. Spectrosc.* **63**, 564–570 (2009).
113. Ali, S.M. *et al.* Raman spectroscopic analysis of human skin tissue sections *ex vivo*: evaluation of the effects of tissue processing and dewaxing. *J. Biomed. Opt.* **18**, 61202 (2013).
114. Mariani, M.M., Lampen, P., Popp, J., Wood, B.R. & Deckert, V. Impact of fixation on *in vitro* cell culture lines monitored with Raman spectroscopy. *Analyst* **134**, 1154–1161 (2009).
115. Deegan, R.D. *et al.* Capillary flow as the cause of ring stains from dried liquid drops. *Nature* **389**, 827–829 (1997).
116. Filik, J. & Stone, N. Analysis of human tear fluid by Raman spectroscopy. *Anal. Chim. Acta* **616**, 177–184 (2008).
117. Filik, J. & Stone, N. Investigation into the protein composition of human tear fluid using centrifugal filters and drop coating deposition Raman spectroscopy. *J. Raman Spectrosc.* **40**, 218–224 (2009).
118. Bonnier, F., Petitjean, F., Baker, M.J. & Byrne, H.J. Improved protocols for vibrational spectroscopic analysis of body fluids. *J. Biophotonics* **7**, 167–179 (2014).
119. Esmonde-White, K.A., Esmonde-White, F.W., Morris, M.D. & Roessler, B.J. Characterization of biofluids prepared by sessile drop formation. *Analyst* **139**, 2734–2741 (2014).
120. Esmonde-White, K.A., Le Clair, S.V., Roessler, B.J. & Morris, M.D. Effect of conformation and drop properties on surface-enhanced Raman spectroscopy of dried biopolymer drops. *Appl. Spectrosc.* **62**, 503–511 (2008).
121. Byrne, H.J., Sockalingum, G. & Stone, N. in *Biomedical Applications of Synchrotron Infrared Microspectroscopy: A Practical Approach* (ed. Moss, D.) Ch. 4, 105–142 (Royal Society of Chemistry, 2011).
122. Fullwood, L.M. *et al.* Effect of substrate choice and tissue type on tissue preparation for spectral histopathology by Raman microspectroscopy. *Analyst* **139**, 446–454 (2014).
123. Wehbe, K., Filik, J., Frogley, M.D. & Cinque, G. The effect of optical substrates on micro-FTIR analysis of single mammalian cells. *Anal. Bioanal. Chem.* **405**, 1311–1324 (2013).
124. Cui, L., Butler, H.J., Martin-Hirsch, P.L. & Martin, F.L. Aluminium foil as a potential substrate for ATR-FTIR, transflection FTIR or Raman spectrochemical analysis of biological specimens. *Anal. Methods* **8**, 481–487 (2016).
125. Lee, K.-S. & El-Sayed, M.A. Gold and silver nanoparticles in sensing and imaging: sensitivity of plasmon response to size, shape, and metal composition. *J. Phys. Chem. B* **110**, 19220–19225 (2006).
126. Faulds, K., Littleford, R.E., Graham, D., Dent, G. & Smith, W.E. Comparison of surface-enhanced resonance Raman scattering from unaggregated and aggregated nanoparticles. *Anal. Chem.* **76**, 592–598 (2004).
127. Nehl, C.L. & Hafner, J.H. Shape-dependent plasmon resonances of gold nanoparticles. *J. Mater. Chem.* **18**, 2415–2419 (2008).
128. Lewis, I.R. & Edwards, H. *Handbook of Raman Spectroscopy: From the Research Laboratory to the Process Line* (CRC Press, 2001).
129. Liu, Z., Zhao, C., Han, L. & Mo, Y. Study on the configuration and applications of high spectral resolution Raman spectrometer. *Guang Pu Xue Yu Guang Pu Fen Xi* **30**, 567–570 (2010).
130. Wieboldt, D. *Understanding Raman Spectrometer Parameters* http://www.spectroscopyonline.com/understanding-raman-spectrometer-parameters (2010).
131. Wiberley, S.E., Colthup, N.B. & Daly, L.H. *Introduction to Infrared and Raman Spectroscopy* 3rd edn. (Elsevier, 2012).
132. Stone, N., Kendall, C., Smith, J., Crow, P. & Barr, H. Raman spectroscopy for identification of epithelial cancers. *Faraday Discuss.* **126**, 141–157 (2004).
133. Zhang, L. & Henson, M.J. A practical algorithm to remove cosmic spikes in Raman imaging data for pharmaceutical applications. *Appl. Spectrosc.* **61**, 1015–1020 (2007).
134. Lasch, P. Spectral pre-processing for biomedical vibrational spectroscopy and microspectroscopic imaging. *Chemometr. Intell. Lab. Syst.* **117**, 100–114 (2013).
135. Barman, I., Kong, C.-R., Singh, G.P. & Dasari, R.R. Effect of photobleaching on calibration model development in biological Raman spectroscopy. *J. Biomed. Opt.* **16**, 011004 (2011).
136. Trevisan, J., Angelov, P.P., Carmichael, P.L., Scott, A.D. & Martin, F.L. Extracting biological information with computational analysis of Fourier-transform infrared (FTIR) biospectroscopy datasets: current practices to future perspectives. *Analyst* **137**, 3202–3215 (2012).
137. Naumann, D. in *Biomedical Optical Spectroscopy, Proceedings of SPIE* (Biomedical Optical Spectroscopy 68530G) (International Society for Optics and Photonics, 2008).
138. Jolliffe, I. *Principal Component Analysis* (Wiley Online Library, 2002).
139. Chen, G. & Shen-En, Q. Denoising of hyperspectral imagery using principal component analysis and wavelet shrinkage. *IEEE Geosci. Remote Sens. Soc.* **49**, 973–980 (2011).
140. Lieber, C.A. & Mahadevan-Jansen, A. Automated method for subtraction of fluorescence from biological Raman spectra. *Appl. Spectrosc.* **57**, 1363–1367 (2003).
141. Mazet, V., Carteret, C., Brie, D., Idier, J. & Humbert, B. Background removal from spectra by designing and minimising a non-quadratic cost function. *Chemometr. Intell. Lab. Syst.* **76**, 121–133 (2005).
142. Savitzky, A. & Golay, M.J.E. Smoothing and differentiation of data by simplified least squares procedures. *Anal. Chem.* **36**, 1627–1639 (1964).
143. Bocklitz, T., Walter, A., Hartmann, K., Rösch, P. & Popp, J. How to pre-process Raman spectra for reliable and stable models? *Anal. Chim. Acta* **704**, 47–56 (2011).
144. Heraud, P., Wood, B.R., Beardall, J. & McNaughton, D. Effects of pre-processing of Raman spectra on *in vivo* classification of nutrient status of microalgal cells. *J. Chemometr.* **20**, 193–197 (2006).
145. Trevisan, J. *et al.* Measuring similarity and improving stability in biomarker identification methods applied to Fourier-transform infrared (FTIR) spectroscopy. *J. Biophotonics* **7**, 254–265 (2014).
146. de Sousa Marques, A., de Melo, M.C.N., Cidral, T.A. & de Lima, K.M.G. Feature selection strategies for identification of *Staphylococcus aureus* recovered in blood cultures using FT-IR spectroscopy successive projections algorithm for variable selection: a case study. *J. Microbiol. Methods* **98**, 26–30 (2014).
147. Lasch, P., Haensch, W., Naumann, D. & Diem, M. Imaging of colorectal adenocarcinoma using FT-IR microspectroscopy and cluster analysis. *Biochim. Biophys. Acta* **1688**, 176–186 (2004).
148. Ellis, D.I. & Goodacre, R. Metabolic fingerprinting in disease diagnosis: biomedical applications of infrared and Raman spectroscopy. *Analyst* **131**, 875–885 (2006).
149. Lloyd, G.R. *et al.* Utilising non-consensus pathology measurements to improve the diagnosis of oesophageal cancer using a Raman spectroscopic probe. *Analyst* **139**, 381–388 (2014).
150. Balabin, R.M., Safieva, R.Z. & Lomakina, E.I. Near-infrared (NIR) spectroscopy for motor oil classification: from discriminant analysis to support vector machines. *Microchem. J.* **98**, 121–128 (2011).
151. Beleites, C., Neugebauer, U., Bocklitz, T., Krafft, C. & Popp, J. Sample size planning for classification models. *Anal. Chim. Acta* **760**, 25–33 (2013).
152. Esbensen, K.H. & Geladi, P. Principles of proper validation: use and abuse of re-sampling for validation. *J. Chemometr.* **24**, 168–187 (2010).
153. Antonio, K.A. & Schultz, Z.D. Advances in biomedical Raman microscopy. *Anal. Chem.* **86**, 30–46 (2013).
154. Parekh, S.H., Lee, Y.J., Aamer, K.A. & Cicerone, M.T. Label-free cellular imaging by broadband coherent anti-Stokes Raman scattering microscopy. *Biophys. J.* **99**, 2695–2704 (2010).
155. Zumbusch, A., Holtom, G.R. & Xie, X.S. Three-dimensional vibrational imaging by coherent anti-Stokes Raman scattering. *Phys. Rev. Lett.* **82**, 4142–4145 (1999).
156. Krafft, C., Dietzek, B. & Popp, J. Raman and CARS microspectroscopy of cells and tissues. *Analyst* **134**, 1046–1057 (2009).
157. Evans, C.L. *et al.* Chemical imaging of tissue *in vivo* with video-rate coherent anti-Stokes Raman scattering microscopy. *Proc. Natl. Acad. Sci. USA* **102**, 16807–16812 (2005).
158. Le, T.T., Huff, T.B. & Cheng, J.-X. Coherent anti-Stokes Raman scattering imaging of lipids in cancer metastasis. *BMC Cancer* **9**, 42 (2009).
159. Gao, L. *et al.* Label-free high-resolution imaging of prostate glands and cavernous nerves using coherent anti-Stokes Raman scattering microscopy. *Biomed. Opt. Express* **2**, 915–926 (2011).
160. Garrett, N. *et al.* Label-free imaging of polymeric nanomedicines using coherent anti-stokes Raman scattering microscopy. *J. Raman Spectrosc.* **43**, 681–688 (2012).
161. Windbergs, M. *et al.* Chemical imaging of oral solid dosage forms and changes upon dissolution using coherent anti-Stokes Raman scattering microscopy. *Anal. Chem.* **81**, 2085–2091 (2009).
162. Schuster, K.C., Reese, I., Urlaub, E., Gapes, J.R. & Lendl, B. Multidimensional information on the chemical composition of single bacterial cells by confocal Raman microspectroscopy. *Anal. Chem.* **72**, 5529–5534 (2000).
163. Majzner, K. *et al.* 3D confocal Raman imaging of endothelial cells and vascular wall: perspectives in analytical spectroscopy of biomedical research. *Analyst* **138**, 603–610 (2012).
164. Caspers, P.J., Lucassen, G.W. & Puppels, G.J. Combined *in vivo* confocal Raman spectroscopy and confocal microscopy of human skin. *Biophys. J.* **85**, 572–580 (2003).

165. Choi, J. *et al.* Direct observation of spectral differences between normal and basal cell carcinoma (BCC) tissues using confocal Raman microscopy. *Biopolymers* **77**, 264–272 (2005).
166. Yu, C., Gestl, E., Eckert, K., Allara, D. & Irudayaraj, J. Characterization of human breast epithelial cells by confocal Raman microspectroscopy. *Cancer Detect. Prev.* **30**, 515–522 (2006).
167. Haka, A.S. *et al.* Identifying microcalcifications in benign and malignant breast lesions by probing differences in their chemical composition using Raman spectroscopy. *Cancer Res.* **62**, 5375–5380 (2002).
168. Breitenbach, J., Schrof, W. & Neumann, J. Confocal Raman-spectroscopy: analytical approach to solid dispersions and mapping of drugs. *Pharm. Res.* **16**, 1109–1113 (1999).
169. Franzen, L., Selzer, D., Fluhr, J.W., Schaefer, U.F. & Windbergs, M. Towards drug quantification in human skin with confocal Raman microscopy. *Eur. J. Pharm. Biopharm* **84**, 437–444 (2013).
170. Skoulika, S.G. & Georgiou, C.A. Rapid quantitative determination of ciprofloxacin in pharmaceuticals by use of solid-state FT-Raman spectroscopy. *Appl. Spectrosc.* **55**, 1259–1265 (2001).
171. Edwards, H., Farwell, D. & Webster, D. FT Raman microscopy of untreated natural plant fibres. *Spectrochim. Acta A Mol. Biomol. Spectrosc.* **53A**, 2383–2392 (1997).
172. Morris, M.D. *et al.* Kerr-gated time-resolved Raman spectroscopy of equine cortical bone tissue. *J. Biomed. Opt.* **10**, 14014 (2005).
173. Prieto, M.C.H. *et al.* Use of picosecond Kerr-gated Raman spectroscopy to suppress signals from both surface and deep layers in bladder and prostate tissue. *J. Biomed. Opt.* **10**, 44006 (2005).
174. Baker, R. *et al.* Depth profiling of calcifications in breast tissue using picosecond Kerr-gated Raman spectroscopy. *Analyst* **132**, 48–53 (2007).
175. Galvis, L., Dunlop, J.W.C., Duda, G., Fratzl, P. & Masic, A. Polarized Raman anisotropic response of collagen in tendon: towards 3D orientation mapping of collagen in tissues. *PLoS ONE* **8**, e63518 (2013).
176. Brose, K., Zouni, A., Broser, M., Müh, F. & Maultzsch, J. Polarised Raman measurements on the core complex of crystallised photosystem II. *Phys. Status Solidi* **246**, 2813–2816 (2009).
177. Blanch, E.W. *et al.* Is polyproline II helix the killer conformation? a Raman optical activity study of the amyloidogenic prefibrillar intermediate of human lysozyme. *J. Mol. Biol.* **301**, 553–563 (2000).
178. McColl, I.H. *et al.* A new perspective on β-sheet structures using vibrational Raman optical activity: from poly(l-lysine) to the prion protein. *J. Am. Chem. Soc.* **125**, 10019–10026 (2003).
179. Blanch, E.W., Hecht, L. & Barron, L.D. Vibrational Raman optical activity of proteins, nucleic acids, and viruses. *Methods* **29**, 196–209 (2003).
180. Nieto-Ortega, B. *et al.* Raman optical activity spectra and conformational elucidation of chiral drugs. The case of the antiangiogenic aeroplysinin-1. *J. Phys. Chem. A* **115**, 2752–2755 (2011).
181. Yamamoto, S., Watarai, H. & Bouř, P. Monitoring the backbone conformation of valinomycin by Raman optical activity. *Chemphyschem* **12**, 1509–1518 (2011).
182. Robert, B. Resonance Raman spectroscopy. *Photosynth. Res.* **101**, 147–155 (2009).
183. Wood, B.R., Caspers, P., Puppels, G.J., Pandiancherri, S. & McNaughton, D. Resonance Raman spectroscopy of red blood cells using near-infrared laser excitation. *Anal. Bioanal. Chem.* **387**, 1691–1703 (2007).
184. Darvin, M. *et al.* Non-invasive *in vivo* detection of the carotenoid antioxidant substance lycopene in the human skin using the resonance Raman spectroscopy. *Laser Phys. Lett.* **3**, 460–463 (2006).
185. Xie, C. & Li, Y.-q. Confocal micro-Raman spectroscopy of single biological cells using optical trapping and shifted excitation difference techniques. *J. Appl. Phys.* **93**, 2982–2986 (2003).
186. Sowoidnich, K. & Kronfeldt, H.-D. Fluorescence rejection by shifted excitation Raman difference spectroscopy at multiple wavelengths for the investigation of biological samples. *ISRN Spectrosc.* **2012**, 1–11 (2012).
187. da Silva Martins, M.A. *et al.* Shifted-excitation Raman difference spectroscopy for *in vitro* and *in vivo* biological samples analysis. *Biomed. Opt. Express* **1**, 617–626 (2010).
188. Matousek, P. & Stone, N. Prospects for the diagnosis of breast cancer by noninvasive probing of calcifications using transmission Raman spectroscopy. *J. Biomed. Opt.* **12**, 024008 (2007).
189. Keller, M.D. *et al.* Development of a spatially offset Raman spectroscopy probe for breast tumor surgical margin evaluation. *J. Biomed. Opt.* **16**, 077006 (2011).
190. Matousek, P. *et al.* Noninvasive Raman spectroscopy of human tissue *in vivo*. *Appl. Spectrosc.* **60**, 758–763 (2006).
191. Olds, W.J. *et al.* Spatially offset Raman spectroscopy (SORS) for the analysis and detection of packaged pharmaceuticals and concealed drugs. *Forensic Sci. Int.* **212**, 69–77 (2011).
192. Stone, N. *et al.* Surface enhanced spatially offset Raman spectroscopic (SESORS) imaging–the next dimension. *Chem. Sci.* **2**, 776–780 (2011).
193. Ma, K. *et al. In vivo*, transcutaneous glucose sensing using surface-enhanced spatially offset Raman spectroscopy: multiple rats, improved hypoglycemic accuracy, low incident power, and continuous monitoring for greater than 17 days. *Anal. Chem.* **83**, 9146–9152 (2011).
194. Yuen, J.M., Shah, N.C., Walsh, J.T. Jr., Glucksberg, M.R. & Van Duyne, R.P. Transcutaneous glucose sensing by surface-enhanced spatially offset Raman spectroscopy in a rat model. *Anal. Chem.* **82**, 8382–8385 (2010).
195. Xie, H.N. *et al.* Tracking bisphosphonates through a 20 mm thick porcine tissue by using surface-enhanced spatially offset Raman spectroscopy. *Angew. Chem.* **124**, 8637–8639 (2012).
196. Sharma, B., Ma, K., Glucksberg, M.R. & Van Duyne, R.P. Seeing through bone with surface-enhanced spatially offset Raman spectroscopy. *J. Am. Chem. Soc.* **135**, 17290–17293 (2013).
197. Saar, B.G. *et al.* Label-free, Real-time monitoring of biomass processing with stimulated Raman scattering microscopy. *Angew. Chem. Int. Ed.* **49**, 5476–5479 (2010).
198. Littlejohn, G.R. *et al. In vivo* chemical and structural analysis of plant cuticular waxes using stimulated Raman scattering (SRS) microscopy. *Plant Physiol.* **168**, 18–28 (2015).
199. Kneipp, K. *et al.* Single molecule detection using surface-enhanced Raman scattering (SERS). *Phys. Rev. Lett.* **78**, 1667–1670 (1997).
200. Nie, S. & Emory, S.R. Probing single molecules and single nanoparticles by surface-enhanced Raman scattering. *Science* **275**, 1102–1106 (1997).
201. Qian, X. *et al. In vivo* tumor targeting and spectroscopic detection with surface-enhanced Raman nanoparticle tags. *Nat. Biotechnol.* **26**, 83–90 (2008).
202. Kneipp, K., Kneipp, H. & Kneipp, J. Surface-enhanced Raman scattering in local optical fields of silver and gold nanoaggregates from single-molecule Raman spectroscopy to ultrasensitive probing in live cells. *Acc. Chem. Res.* **39**, 443–450 (2006).
203. Cîntă Pînzaru, S., Pavel, I., Leopold, N. & Kiefer, W. Identification and characterization of pharmaceuticals using Raman and surface-enhanced Raman scattering. *J. Raman Spectrosc.* **35**, 338–346 (2004).
204. Huang, X., El-Sayed, I.H., Qian, W. & El-Sayed, M.A. Cancer cells assemble and align gold nanorods conjugated to antibodies to produce highly enhanced, sharp, and polarized surface Raman spectra: A potential cancer diagnostic marker. *Nano Lett.* **7**, 1591–1597 (2007).
205. Feng, S. *et al.* Nasopharyngeal cancer detection based on blood plasma surface-enhanced Raman spectroscopy and multivariate analysis. *Biosens. Bioelectron.* **25**, 2414–2419 (2010).
206. Premasiri, W. *et al.* Characterization of the surface enhanced Raman scattering (SERS) of bacteria. *J. Phys. Chem. B* **109**, 312–320 (2005).
207. Zeiri, L. SERS of plant material. *J. Raman Spectrosc.* **38**, 950–955 (2007).
208. McNay, G., Eustace, D., Smith, W.E., Faulds, K. & Graham, D. Surface-enhanced Raman scattering (SERS) and surface-enhanced resonance Raman scattering (SERRS): a review of applications. *Appl. Spectrosc.* **65**, 825–837 (2011).
209. Graham, D. *et al.* Selective detection of deoxyribonucleic acid at ultralow concentrations by SERRS. *Anal. Chem.* **69**, 4703–4707 (1997).
210. Murgida, D.H. & Hildebrandt, P. Electron-transfer processes of cytochrome *c* at interfaces. New insights by surface-enhanced resonance Raman spectroscopy. *Acc. Chem. Res.* **37**, 854–861 (2004).
211. Murgida, D.H. & Hildebrandt, P. Disentangling interfacial redox processes of proteins by SERR spectroscopy. *Chem. Soc. Rev.* **37**, 937–945 (2008).
212. Böhme, R. *et al.* Biochemical imaging below the diffraction limit–probing cellular membrane related structures by tip-enhanced Raman spectroscopy (TERS). *J. Biophotonics* **3**, 455–461 (2010).
213. Stone, N. & Matousek, P. Advanced transmission Raman spectroscopy: a promising tool for breast disease diagnosis. *Cancer Res.* **68**, 4424–4430 (2008).
214. Johansson, J., Sparén, A., Svensson, O., Folestad, S. & Claybourn, M. Quantitative transmission Raman spectroscopy of pharmaceutical tablets and capsules. *Appl. Spectrosc.* **61**, 1211–1218 (2007).
215. Buckley, K. & Matousek, P. Recent advances in the application of transmission Raman spectroscopy to pharmaceutical analysis. *J. Pharm. Biomed. Anal.* **55**, 645–652 (2011).